The Pennsylvania State University

The Graduate School

LEAD ZIRCONATE TITANATE MICROSPHERES

FOR

ULTRASONIC APPLICATIONS

A Thesis in

Ceramic Science

by

Dean R. Smith

Submitted in Partial Fulfillment
of the Requirements
for the Degree of

Master of Science

May 1995

We approve the thesis of Dean R. Smith.

Date of Signature

April 28, 1995

Susan Trolier-McKinstry
Assistant Professor of Ceramic Science
and Engineering
Thesis Advisor

April 28, 1995

Kenji Uchino
Professor of Electrical Engineering

April 28, 1995

Darrell Schlom
Assistant Professor of Materials Science
and Engineering

April 27, 1995

David J. Green
Professor of Ceramic Science and Engineering
In Charge of Graduate Programs in
Ceramic Science

ABSTRACT

Lead zirconate titanate microsphere transducers have been successfully fabricated and characterized to evaluate their potential for use as hydrophones and in biomedical ultrasound applications. The fabrication procedure is described and a statistical sphere evaluation is presented. It was found that improvements in the wall thickness variation and wall density of the spheres will be of utmost importance to achieve further improvements in the spheres' transducer properties. Characterization of the spheres consisted of dielectric, piezoelectric, hydrostatic, and submerged impulse response testing. The average dielectric constant of the spheres is low, however, d_h values of up to 1000 pC/N have been measured. This value is approaching that of the well-known moonie actuators. Pulse - echo response plots are also included for the spherical transducers. Bandwidths of up to 79% were obtained, which makes the spheres good candidates for ultrasonic imaging transducers when optimized with backing and matching layers.

TABLE OF CONTENTS

LIST OF TABLES

LIST OF FIGURES

ACKNOWLEDGMENTS

I would like to extend a world of thanks to my academic and research advisor, Dr. Robert E. Newnham, for giving me the opportunity to work and learn under his supervision, but mostly for his patience and guidance throughout my stay at Penn State and the MRL.

I would like to extend a great deal of thanks to Dr. Susan Trolier-McKinstry for accepting the responsibility as my thesis advisor and faithfully motivating me through the completion of this project, even when the situation appeared bleak. Without her assistance this thesis would not be finished at this time.

I would also like to thank Dr. Darrell Schlom and Dr. Kenji Uchino for their helpful inputs and for serving as my committee members.

I would like to extend my appreciation to Shoko Yoshikawa and Dr. Joseph Fielding for assisting in the coordination of this project, and for all of their guidance.

Special thanks go out to my friends Richard Meyer, Jr., Michael Woolfolk, James Tressler, and Aydin Dogan for always being there when times got tough.

For fear of missing anyone, I would like to extend a thank you to the entire staff of MRL for all of their assistance, inputs, and guidance; which was considerable. (We miss you: Judy Marks!)

I would like to thank Arthur Balotto and the Army Research office for supporting this research. Without such support this project would have never been possible.

Lastly, I would like to give special thanks and acknowledgment to my wonderful parents and family whose support has been rock solid through it all. Well, Mom and Dad; it looks like we made it through another one!

CHAPTER 1

INTRODUCTION/OBJECTIVES

Soon after they were discovered, piezoelectric ceramics were noted for their usefulness as transducers for sensors and actuators, such as micropositioners, pressure sensors, and ultrasound generators. For many years, considerable research in piezoceramics was carried out to discover compositions which would provide optimum properties for specific applications. It was through this research that PZT (Lead Zirconate Titanate) was discovered. It was found that PZT has a morphotropic phase boundary at a zirconium:titanium ratio of 52:48 (Jaffe et al., 1971). For compositions at or near this phase boundary, the dielectric and piezoelectric properties and the electromechanical coupling coefficients increase considerably. It is for this reason that PZT is the most widely used transducer material today.

Recently, there has been a shift in the direction of research for piezoelectric ceramics towards development of novel device geometries. Towards this end, this thesis explores the use of miniature PZT hollow spheres as a new type of piezoelectric transducer.

1.1 BACKGROUND

Much of the current research in transducer design is focused on novel ways to combine piezoelectric ceramics with other materials to form composites which possess optimum properties for a given application. A typical example of this is the piezo-composite panels developed for sonar and active surface control applications which utilize 1-3 connectivity to optimize their performance (Gentilman et al., 1995).

Another area where significant improvements are being made is in the design of the active piezoelectric sensor elements. By utilizing clever element designs, researchers have been able to improve the performance of transducers in applications such as biomedical ultrasound and underwater hydrophone systems. These systems are described further in Section 1.3 of this chapter.

Miniature PZT hollow sphere transducers, recently developed at the Pennsylvania State University Materials Research Laboratory, show a combination of useful transducer properties (Meyer, Jr. et al., 1994). In previous work, properties such as the dielectric constant, coupling coefficients, and piezoelectric constants were calculated and measured. The preliminary results from this study are described later in this section.

This thesis is a further investigation of the piezoelectric microspheres, to evaluate their potential for use in applications where other devices are currently being used.

1.2 OBJECTIVES

The objective of this study is to evaluate the feasibility of producing a large number of spherical transducers with reproducible properties, and to optimize the properties of the PZT spheres. A number of avenues need to be addressed to complete the investigation. A test to remove defective spheres with holes or cracks to "weed" them out before going through the fabrication process is needed. A complete statistical evaluation of the spheres is necessary in order to track reproducibility data on the spheres from the as-received condition through the fabrication processes to obtain yield data. Optimization of the burnout and sintering schedules needs to be addressed through evaluation of stoichiometry and lead loss. Each procedure in the fabrication process should be evaluated to develop improved properties and/or to facilitate the mass production of transducers with reproducible properties. Finally, the spheres will be characterized and dielectric, piezoelectric, hydrostatic, and impulse response testing will be completed and reported.

1.3 APPLICATIONS

1.3.1 Introduction

Two immediate potential applications become apparent when looking for areas in which PZT hollow sphere transducers may aid in the effectiveness of current sensor systems. These applications are biomedical ultrasound and underwater hydrophone systems. The small size and spherical geometry of the spheres which can be produced by the Torobin process are expected to provide improvements in image resolution and beacon location in biomedical ultrasound applications, and expand the frequency range of underwater spherical hydrophones. A thorough study on the effect of acoustic matching and backing layers to improve the acoustic impedance mismatch between ultrasonic transducers and the surrounding media has been completed (Grewe, 1989), which provided insight for future improvements in the spherical transducers' performance.

Ultrasonic imaging requires the transfer of energy between media of different densities. As the ultrasonic wave reaches a boundary of media with differing densities, some of the energy will be transmitted through the boundary and some of the energy will be reflected as shown in Figure 1.1. The efficiency of the transfer of energy through the boundary is largely determined by the acoustic impedance mismatch between the two media. The acoustic impedance (Z) of a material is determined by:

$$Z(Rayl) = c_l \rho \qquad \text{Equation 1.1}$$

where c_l is the velocity of the longitudinal sound wave and ρ is the density of the medium. c_l is determined by:

$$c_l = \left(\frac{K}{\rho}\right)^{0.5}$$

Equation 1.2

where K is the bulk modulus and ρ is the density of the medium (Silk, 1984).

The average effective density of the sealed PZT spheres studied in the current work is just over 1.0 g/cm^3. The close density match between the spherical sensor and the surrounding media (the density of water = 1.0 g/cm^3 and human tissue is nearly 1.0 g/cm^3) should reduce the coupling losses and the acoustic impedance mismatch, and therefore improve the efficiency of the energy transfer through the medium.

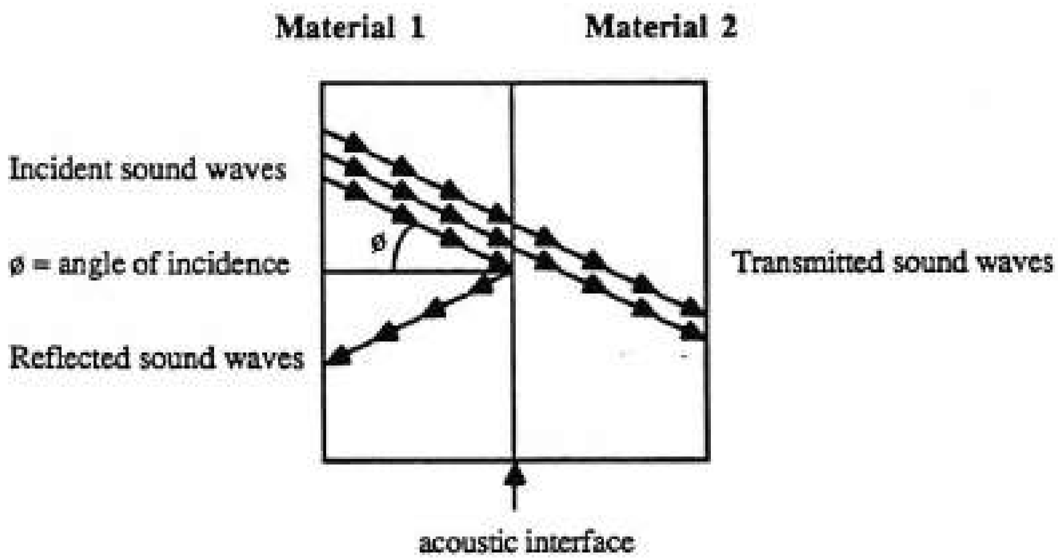

Figure 1.1

Transmission/Reflection Wave Phenomena at the Interface of Media with Differing Densities (Grewe, 1989)

The PZT spheres under investigation in this thesis are similar in size to spherical transducers which are fabricated by coating a small brass bead with a thin layer of PVDF (Poly Vinylidene Di-Fluoride) for use as guidance beacons in angioplasty operations (Vilkomerson et al., 1992). Transducers with spherical geometry are desirable for use as guidance beacons due to their omnidirectional characteristics. Before this study, fabrication limitations were most likely the main reason why PZT spherical sensors were not considered for this application. We feel that the new fabrication methods may allow PZT spheres to be utilized for *in-vivo* guidance applications.

The Naval Research Laboratory has developed a series of spherical omnidirectional underwater hydrophones for use as calibrated standards, the smallest of which is in the 1 cm size range (Ivey, 1979). Romanenko (1957) reported that in order to measure turbulent flow near an underwater surface it is desirable to utilize omnidirectional sensors with dimensions smaller than the wavelengths of the incoming acoustic waves. This implies that smaller hydrophones are likely to achieve better resolution of flow noise and improve their ability to detect small objects. Therefore, the millimeter sized PZT spheres in this investigation may also be useful in improving the resolution limitation inherent in the larger hydrophones which are used by the Navy.

The spheres can also be mounted easily into arrays to be used as a transducer for non-destructive testing and non-destructive evaluation techniques. Figure 1.2 displays what a typical simple array might look like.

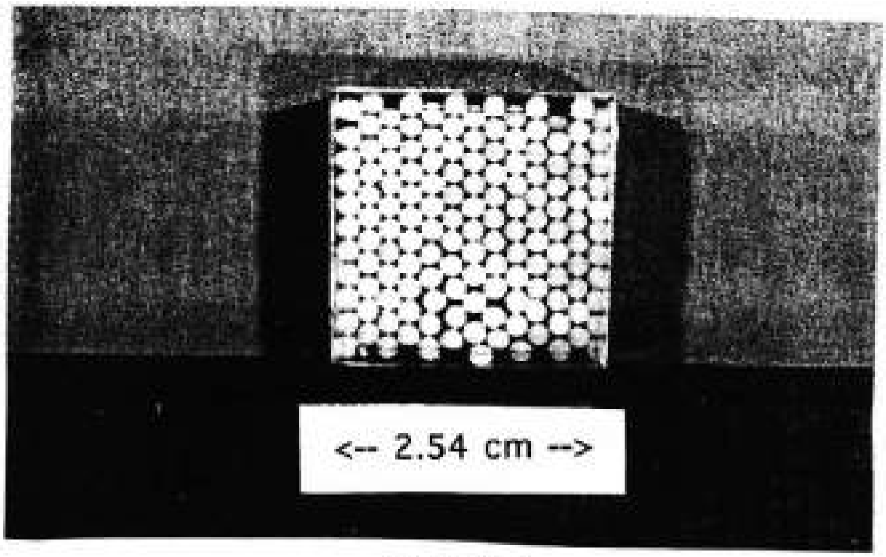

Figure 1.2

Typical Simple Array (from Meyer, Jr. et al., 1994)

1.3.2 Ultrasonic Image Catheters

Ultrasonic image catheters (UIC's) are primarily used in medical ultrasound applications for two applications: as guidance systems on catheters (Neville et al., 1989), and for inspection of arterial walls (atherosclerosis) (Meyer et al., 1988). UIC's are already used in balloon angioplasty procedures, in which small catheters are used to direct an inflatable balloon to dilate a narrowed blood vessel. Imaging of internal organs through the use of small invasive devices is also under development. The use of UIC devices eliminates dissection of large areas of the body, typical in conventional surgery. A small incision is made and the catheter is guided through the body to complete the surgery, utilizing ultrasonic images. This method reduces the risk of infection, trauma, surgical costs, and the length of hospital visits (Vilkomerson et al., 1992).

Other alternatives to UICs used to guide catheters are X-ray fluoroscopy and fiber optic angioscopes (Pandian et al., 1989). X-ray fluoroscopy utilizes x-rays along with a dye material, both of which are potentially harmful to the human body. Fiber optic angioscopes have short-comings in evaluating wall thickness and vessel structure associated with artery diagnosis. UICs are being developed to eliminate these deficiencies.

Ultrasonic imaging utilizes the Pulse-Echo method to achieve images within the body. The method is coined "Pulse-Echo" because the same transducer is used to transmit and receive the ultrasonic waves. The transducer is excited with a short electrical impulse, which sends an ultrasonic wave into the surrounding media. As the wave travels through tissues of differing densities, part of the wave is reflected back toward the sensor as described earlier. The time delay of the reflected waves, produced by the tissues of differing densities, is proportional to their distance from the transducer. The echoed waves return to the transducer, where the energy is converted back to electrical impulses. A transfer function of the electrical signals is generated which allows the image to be displayed on a CRT screen utilizing complicated algorithms (Wells, 1977) and (Gururaja, 1989). A typical ultrasonic image of a human vein is shown in Figure 1.3.

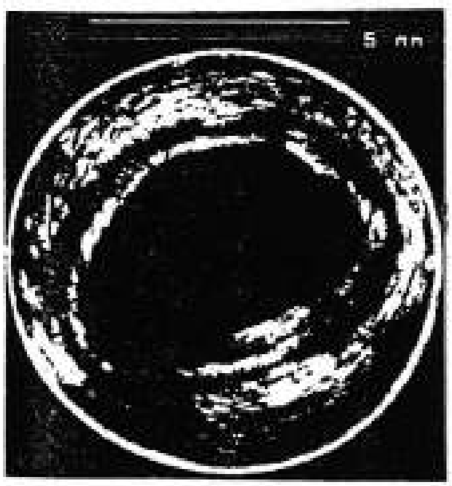

Figure 1.3

UIC Image of a Vein Cross Section

(from Meyer, et al., 1989)

Piezoelectric material properties are important factors to consider when utilizing ultrasound. Many piezoelectric materials have been investigated, but PZT and PVDF are the most widely used. For optimal performance in *in-vivo* imaging and guidance the transducers must be small, have low insertion loss, possess a wide working frequency range, have a high dielectric constant, a large electromechanical coupling coefficient, and appropriate directionality (Neville, et al., 1989). PZT meets most of these requirements, although it is not easy to fabricate the ceramic in small sizes or in the necessary shapes. An even greater shortcoming of bulk PZT is the high acoustic impedance mismatch with tissue and water. The coupling coefficient, k_t, and the insertion loss are considered the two most important criteria in evaluating transducer performance in the frequency range of interest. Small transducers capable of operating in the 1-100 MHz frequency range are necessary to evaluate narrow blood vessels. Normally, center frequencies of 5-20 MHz are used for imaging cardiac structures, and 20-40 MHz for imaging the smaller vessels (Pandian, 1989). In this range, the insertion loss is reduced by reducing acoustic impedance mismatch between the transducer and the surrounding tissue. The acoustic impedance of PZT is ~ 30 MRayl, whereas water and tissue are ~1.5 MRayl. The hollow PZT spheres described in this thesis exhibit about the same impedance as PVDF: ~ 4 MRayl. Thus from the standpoint of insertion loss, PZT spheres should perform better than monolithic PZT sensors.

In UIC applications, omnidirectional sensors hold an advantage over traditional cylindrical and disc-shaped sensors because they are capable of receiving and transmitting signals at angles up to almost 360°. This allows the sensor to "see" and "hear" behind itself, and achieve accurate locations even when the sensor is moving in a direction that is not perpendicular to the scan head. A catheter guidance system now on the market, made by Echomark Catheter Technology Company, is shown in Figure 1.4. This system utilizes a PVDF omnidirectional transducer. The transducer is made by depositing a 70 μm thick layer of PVDF onto a 2.5 mm diameter brass sphere (Cluely et al., 1991). This system not only provides accurate echo location, but also is capable of imaging balloon dilation during angioplasty procedures. PZT hollow sphere transducers can operate in the same frequency range as PVDF, but hold the advantage of significantly higher electromechanical coupling coefficients.

Another type of UIC, known as a diagnostic catheter, is shown in Figure 1.5. This catheter is useful for obtaining a cross-sectional image of a blood vessel by rotating the sensor 360° either manually or mechanically. Center frequencies of 20-25 MHz are used. Hemispherical-disk shaped transmitters, cut from PZT spheres, may be useful in focusing the beam on diseased tissue in the vascular system.

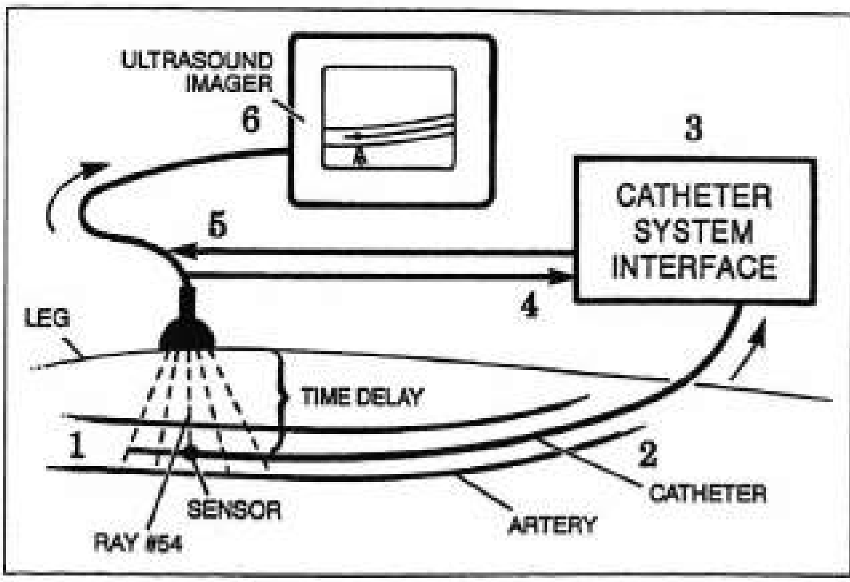

Figure 1. EchoMark ultrasound-guided catheter system. 1. Imaging ultrasound pulse strikes omnidirectional receiver attached to the mid-balloon region of the catheter. 2. Signal is transmitted through wire in catheter to catheter-system interface (CSI). 3. CSI measures time delay for transmission of imaging ultrasound pulse from the scan head to the receiver. 4. CSI determines the particular ultrasound ray (i.e., ray 54) that strikes the receiver by monitoring the transmissions at the scan head. 5. Information tabulated from steps 3 and 4 is used to determine the location of the receiver in the horizontal and vertical planes. This positional information is transmitted from the CSI to the scan head where it is electromagnetically injected into the B-mode image and displayed on the duplex monitor. 6. The location of the receiver is represented by a flashing bright arrow superimposed on the ultrasound B-mode image.

Figure 1.4

Schematic of Echomark Catheter System

(from Cluley et al., 1991)

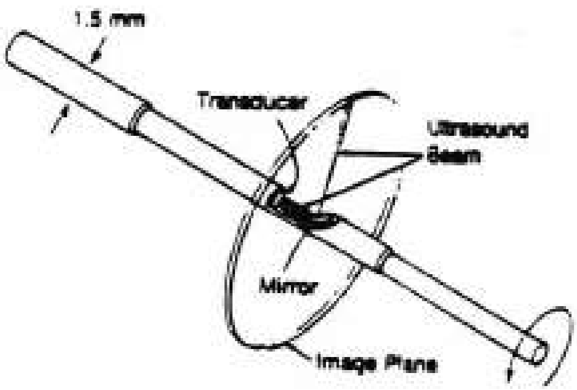

Figure 1.5

Diagnostic Catheter

(from Neville et al., 1989)

1.3.3 Spherical Hydrophones

A series of spherical omnidirectional transducers, the Series F42, was developed at the Underwater Sound Reference Detachment for the Naval Research Laboratory as calibrated standards with omnidirectional radiation patterns to 100 KHz (Ivey, 1979). The series consists of four transducers. Each has the same design, the only difference being size and thus response sensitivity and frequency range. The elements are made of PZT hollow spheres, ranging in size from 1.3 to 5 cm in diameter. The spheres consist of two PZT hemispheres that are epoxied together and are electrically connected in parallel. The connected leads are then brought out through a small hole between the hemispheres.

The transducers have been designed to act as both transmitters and receivers over the frequency range 1 to 160 KHz. The upper cutoff frequency is attributed to the breathing mode of vibration of the sphere. The frequency of the tiny spheres discussed in this investigation extends this range to ~700 KHz. The outer diameter of the spheres can be selected to achieve a desired frequency range.

The free-field voltage sensitivity of the piezoelectric hollow spheres can be calculated by (Ivey, 1979):

$$\frac{V}{P_o} = \frac{b}{c^2 + c + 1}\left[g_{33}\left(\frac{c^2 + c - 2}{2}\right) - g_{31}\left(\frac{c^2 + c + 4}{2}\right)\right] \qquad \text{Equation 1.3}$$

where V is the open circuit voltage developed by the sensor, P_0 is the external pressure in N/m^2, c = a/b, and a and b are the inner and outer radii of the sphere expressed in meters, g_{33} and g_{31} are the piezoelectric voltage coefficients of the poled ceramic measured in units of volt-meters per Newton. A list of free-field voltage sensitivities (units: dB re V/μPa) of the F42 series transducers is provided in Table 1.1. The calculated value for the tiny PZT spheres described in this report is also included for comparison (Model E). The receiving sensitivity of the spheres decreases as the sphere diameter is decreased. Conversely, the resonant frequency increases as the sphere diameter decreases. These characteristics are shown graphically in Figure 1.6. Further reduction in size of the PZT microspheres could extend this response up to ~1 MHz.

The transmitting voltage response (TVR) is another coefficient which describes the effectiveness of a hydrophone. It is usually expressed in terms of pressure/volt at 1 meter, and is determined by (Clancy et al., 1991):

$$TVR = \frac{a' b'^4 \omega^2 P_o \varepsilon_o K_{33}^T}{b'^3 - a'^3}\left[g_{33}\left(\frac{c^2 + c - 2}{2}\right) - g_{31}\left(\frac{c^2 + c + 4}{2}\right)\right] \qquad \text{Equation 1.4}$$

where P_0 is the density of the medium, ω is the angular frequency, and ε_0 the permittivity of free space. K_{33} is the ceramic dielectric constant, and a' and b' are the inner and outer diameters of the sphere.

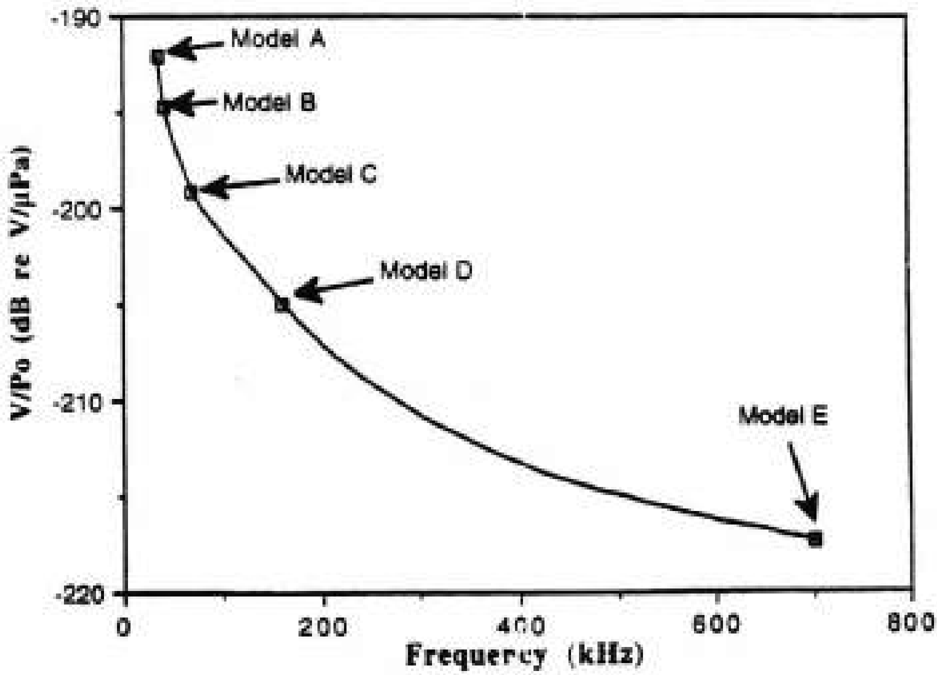

Figure 1.6

Voltage Sensitivity vs. Frequency

Calculated values of TVR for the Navy F42 series are shown in Table 1.1. The value for Model E is also included for comparison. Model E has the lowest TVR, as can be expected from the free-field voltage sensitivity, and the highest frequency range because of its small size.

Table 1.1

Navy Series F42 Data

Parameter	Model A	Model B	Model C	Model D	Model E
Outside Radius (m)	0.025	0.0191	0.0127	0.0064	0.0013
c	0.872	0.832	0.748	0.844	0.931
V/P_o (dB re V/μPa)	-192.05	-194.70	-199.20	-205.00	-217.34
TVR (dB re μPa/V)	125	116	105.4	97.9	80.6

1.4 PRELIMINARY STUDY

A preliminary study on piezoelectric hollow sphere transducers has been reported (Meyer, Jr. et al., 1994). Two transducer configurations were investigated: radially poled and top-to-bottom poled samples. Since the current study focuses on the radially poled transducer's characteristics, we shall not consider the top-to-bottom poling. Calculations and measurements were taken on the spheres' transducer properties. A summary of the results follows.

The expected capacitance of the spheres was calculated using the spherical capacitor model. For the PZT 5 composition used to prepare the spheres in this study the capacitance was calculated to be approximately 3000 pF. However, the typical capacitance measured at 10 KHz and 0.1 V on actual samples was ~900 pF.

The primary mode of vibration of a sphere is the breathing mode. The expected resonant frequency for the thin walled spheres used in this study is calculated to be approximately 600 KHz. A typical measured value for the resonance was found to be 675 KHz.

The secondary mode of vibration in a sphere is the wall thickness mode. The frequency of this mode was calculated, using an average wall thickness of 90 μm, to be 14.5 MHz. Initial measurements yielded an average of approximately 12 MHz.

A typical plot of the breathing and thickness modes is shown in Figure 1.7. It was reported that the resonant frequencies of each mode are reproducible to within ± 5.0 % and can be shifted in frequency by changing the wall thickness and/or the diameter of the spheres.

The planar coupling coefficient (k_p) for the spheres was calculated using the resonant/antiresonant frequency method. Using the values taken from Figure 1.5a the value for k_p is 0.30 from this data. This is significantly smaller than the accepted value of 0.60 for bulk material.

Most of the deviations between the expected values and the measured values of the sphere properties were tied to electroding problems and imperfections in the hollow sphere shape. The discrepancies were also noticed in this study. Detailed discussion on this subject can be found in Chapter 3.

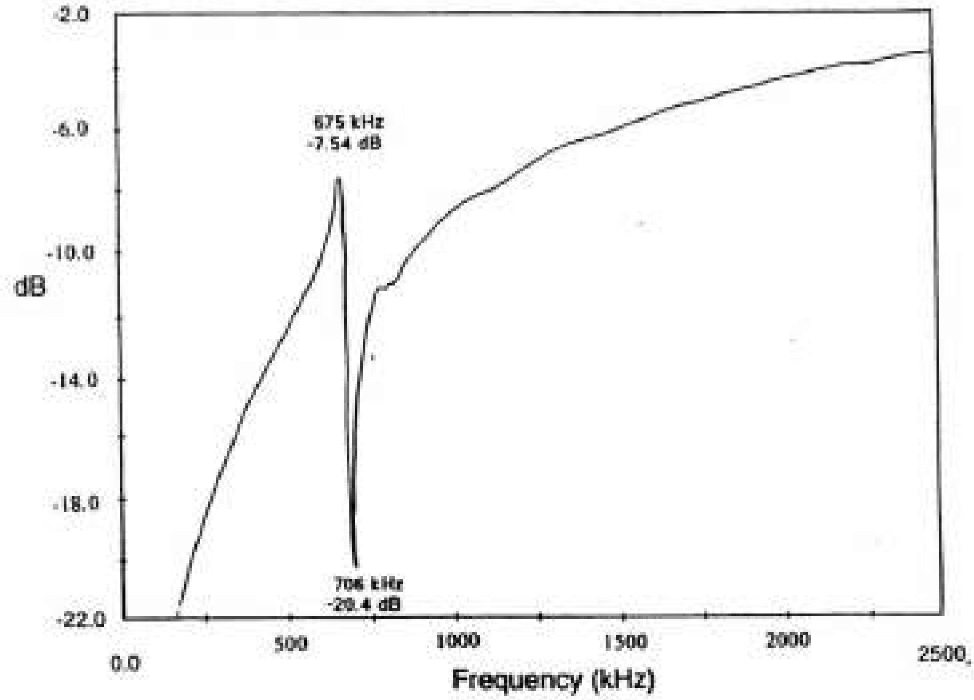

A: Primary Breathing Mode Resonance

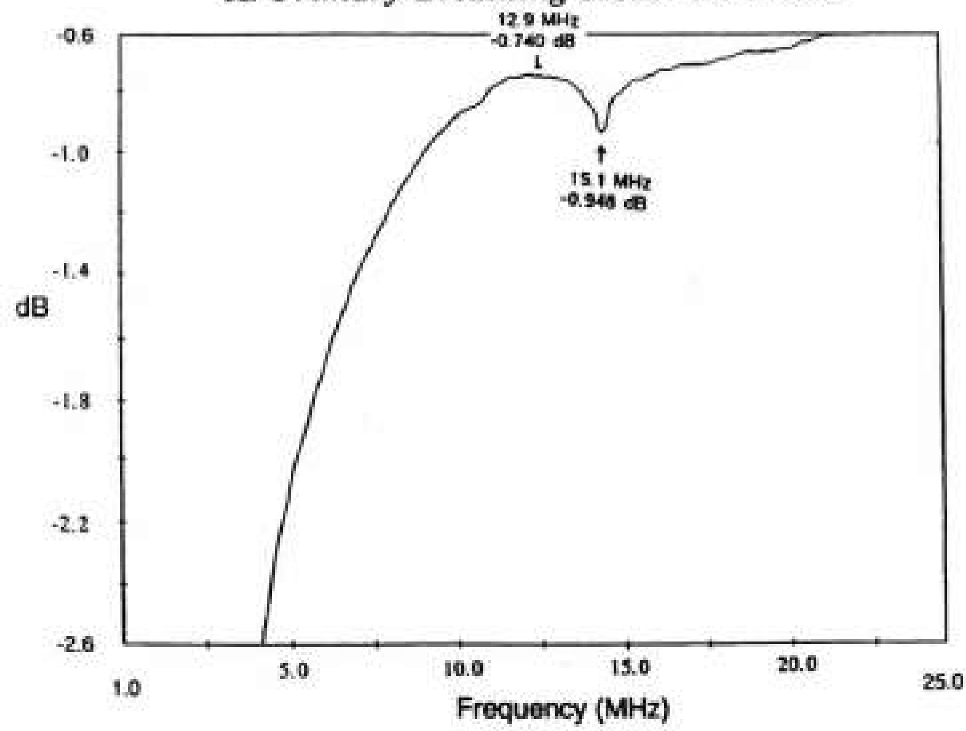

B:Secondary Thickness Mode Resonance

Figure 1.7

Admittance Spectra of the Primary and Secondary

Modes of Vibration (Meyer, Jr. et al., 1994)

CHAPTER 2

EXPERIMENTAL PROCEDURE

2.1 SPHERE FORMATION

A fabrication procedure for producing very high volumes of alumina and mullite hollow spheres has been developed at the Georgia Institute of Technology (Chapman et al., 1987);(Torobin et al., 1991). The initial goal of the project was to produce light weight furnace insulation and other light weight refractory based products by bonding the spheres together to form a ceramic/air composite.

The procedure utilizes a concentric tube arrangement where air is blown through the center tube and a ceramic slurry is forced through the outside tube. A fluid dynamic model for this process describes the stresses on the sphere surfaces as hydrostatic pressures, viscous stresses, and stresses caused by surface tension (Chapman et al., 1991). The equation describing the stress balance for the system is given as:

$$\Delta P + \left(P_{liq,R+w} - P_{liq,R}\right) + \left(\tau_{rr}|_{liq,R}| - \tau_{rr}|_{liq,R+w}|\right) = 2\alpha\left(\frac{1}{R} - \frac{1}{R+w}\right) \qquad \text{Equation 2.1}$$

where:

a = liquid surface tension,

ΔP = pressure difference across the spherical shell,

$P_{liq,R+w}$ = hydrostatic pressure of liquid at outer surface of sphere,

$P_{liq,R}$ = hydrostatic pressure of liquid at inner surface of sphere,

$t_{rr} I_{air,R+w}$ = viscous stress due to atmospheric air,

$t_{rr} I_{liq,R+w}$ = viscous stress due to liquid at outer surface of sphere,

$t_{rr} I_{liq,R}$ = viscous stress due to liquid at inner surface of sphere,

$t_{\pi}I_{gas,R}$ = viscous stress due to gas inside the sphere.

The process was fine tuned to produce a large number of relatively uniform hollow spheres by optimizing processing variables such as the slurry viscosity, flow rates of both air and the slurry, and nozzle dimensions. It was reported that tolerances on the dimensions and weight could be held to less than ± 6% (Chapman et. al., 1991).

It should be noted that the PZT spheres used for this investigation were produced at the Georgia Institute of Technology on the first prototype run ever attempted to form hollow piezoelectric microspheres. Therefore, further improvements and adjustments in the fabrication procedure for producing piezoelectric spheres would more than likely produce spheres with improved dimensional tolerances when compared the ones used for this study.

The process has also been used to produce metal hollow spheres. These may be useful for light weight prototype structural composites for use in aircraft and aerospace applications (Clancy et al., 1991).

2.2 POWDER EVALUATION

The spheres produced for this investigation were fabricated from a slurry of PZT 501A powder (a composition based on doped $Pb(Zr_{0.52}, Ti_{0.48})O_3$), provided by Ultrasonic Powders Inc.: Lot # L-586. A sample of the powder was set aside to be used as a reference to verify the quality of the powder, and to evaluate the dielectric and piezoelectric properties of the bulk material for comparison with the spheres.

2.2.1 Pellet Preparation

The powder was ground with a mortar and pestle and then sieved through a no. 120 (125 μm) mesh to separate any large particles or agglomerates. Three weight percent Acriloid binder (Rohm and Haas) was added and the powder was again ground and sieved.

From this powder, 12.7 mm diameter pellets were pressed in a hydraulic press at 100 MPa. The disk thickness was approximately 1.2 mm. The firing process consisted of a binder burnout at 550°C for one-half hour, followed by sintering at 1285°C for 90 minutes in a lead atmosphere. The lead atmosphere was provided by a mixture of powder, 18 parts PbO to 10 parts ZrO_2 by weight. An alumina boat filled with 1.5 grams of this powder was placed inside the crucible during sintering. The firing schedule was determined as the optimum firing condition through evaluation of an experimental time-temperature matrix which will be discussed subsequently. The pellets were then x-rayed to insure that single phase perovskite was obtained, and then surface ground to a thickness of 1 mm. A typical diffraction pattern can be seen in Figure 2.1. Platinum electrodes were deposited during a 4 minute sputtering step. The pellets were poled with an electric field of 34 KV/cm at 130°C.

2.2.2 Time - Temperature Matrix

A time - temperature matrix (Table 2.1) was investigated to obtain a firing schedule which would provide the best dielectric properties. Several ceramic discs were fired under various conditions in a lead atmosphere, and evaluated to determine an optimum firing schedule for the PZT hollow spheres described in this investigation. The evaluation of the pellets consisted of dielectric and piezoelectric characterization, and is described in the next section.

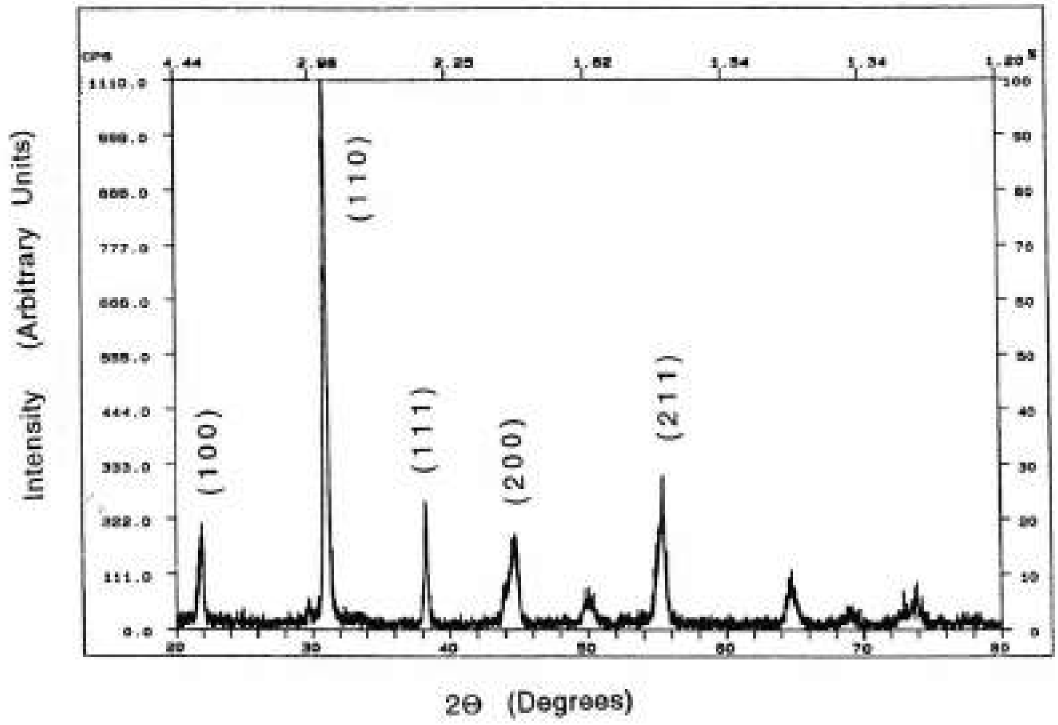

Figure 2.1

Typical Diffraction Pattern of a PZT Pellet

Using Cu Kα Radiation

Table 2.1

Time - Temperature Firing Matrix

1200 °C 45 Min.	1200 °C 90 Min.
1240 °C 45 Min.	1240 °C 90 Min.
1285 °C 45 Min.	1285 °C 90 Min.

2.2.3 PZT Disk Evaluation

(a) Dielectric Measurements

Low frequency dielectric measurements for poled and unpoled disks were obtained using an HP 4274A Multi - Frequency LCR Meter at 10 KHz and 1 V/mm. The data obtained are compiled in Tables 2.2 and 2.3.

Table 2.2

Capacitance and Dielectric Loss of Unpoled Pellets as a Function of the Temperature and Firing Time

Firing Temp / Firing Time	45 Min.	90 Min.	
1200 °C	1044 0.031	1034 0.031	ave. capacitance (pF) ave. loss (tan δ)
1240 °C	984 0.033	970 0.032	
1285 °C	956 0.033	965 0.031	

Table 2.3

Capacitance and Dielectric Loss of Poled Pellets as a Function of the Temperature and Firing Time

Firing Temp / Firing Time	45 Min.	90 Min.	
1200 °C	1400 0.023	1409 0.024	ave. capacitance (pF) ave. loss (tan δ)
1240 °C	1329 0.024	1369 0.023	
1285 °C	1404 0.024	1397 0.023	

From the capacitance values obtained for the time - temperature combinations in the matrix, the dielectric constant, K, for each point in the matrix can be calculated from the equation:

$$C = \frac{\varepsilon_o K A}{t}$$

Equation 2.2

where A is the area, ε_o is the permitivity of free space, and t is the thickness. The calculated values for the average dielectric constant at each matrix point can be seen in Table 2.4.

The average poled dielectric constant for each of the time/temperature points in the matrix was ~1720 ± 36. This agrees relatively well with the value of 1850 specified by Ultrasonic Powders Inc. for PZT 501A powder.

The values for the dielectric constants of the pellets indicated that the powder was of good quality. However, due to the small variance in the data with firing conditions, it was decided that the piezoelectric properties of the material might give more insight in determining an optimum firing schedule.

Table 2.4

Calculated Dielectric Constant

of Poled PZT Disks

Firing Temp / Firing Time	45 Min.	90 Min.
1200 °C	1735	1747
1240 °C	1654	1698
1285 °C	1740	1732

(b)Piezoelectric Measurements

Hysteresis (P-E) Loops

A polarization vs. electric field hysteresis loop was obtained for each pellet to evaluate the remanent polarization (P_r) and the coercive field (E_c) at each time / temperature point in the matrix. A schematic of the experimental setup is shown in Figure 2.2. The driving voltage was increased until P_r reached saturation. The data describing P_r and E_c are shown in Table 2.5.

In general, P_r increased and E_c decreased for longer soaking times and higher temperature firings. The maximum P_r and the minimum E_c occurs at 1285°C for 90 minutes. A typical hysteresis loop from this time / temperature combination is shown in Figure 2.3.

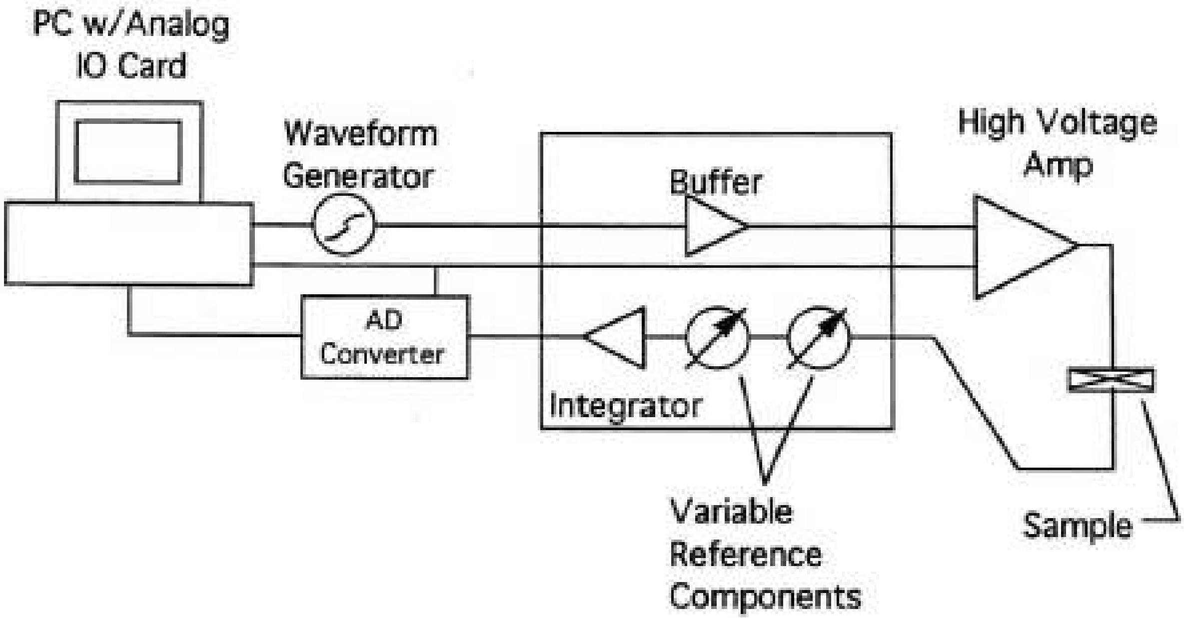

Figure 2.2

Schematic of the Hysteresis Experimental Setup

Table 2.5

Remanent Polarization and Coercive Field

of PZT Disks

Firing Temp / Firing Time	45 Min.	90 Min.
1200 °C	350 1.10	354 1.05
1240 °C	333 1.17	348 1.10
1285 °C	361 1.02	364 0.93

remanent polarization - Pr (mC/m^2)
coercive field - Ec (MV/m)

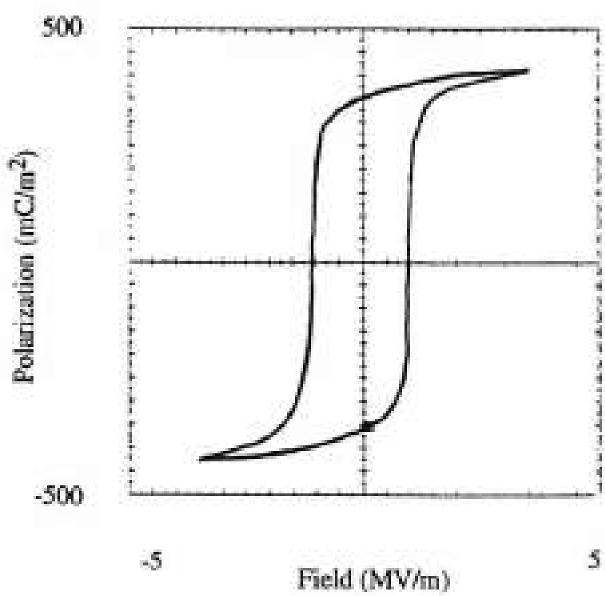

Figure 2.3

Typical Hysteresis Loop for a PZT Pellet

Fired at 1285° C for 90 Minutes

Piezoelectric Constants

Piezoelectric constants (d_{33}) for the pellets were obtained utilizing a Berlincourt Piezo d_{33} Meter (Channel Products, Inc.). The measurements were taken at 100 Hz and with the medium response time setting. The values obtained are shown in Table 2.6.

Table 2.6

Average Piezoelectric (d_{33}) Constants in pC/N

Firing Temp / Firing Time	45 Min.	90 Min.
1200 °C	377	384
1240 °C	386	380
1285 °C	386	395

From the table it can be seen that a firing schedule of 1285 °C for 90 minutes produced the largest average piezoelectric constant (395 pC/N), which is close to that of the manufacturers (UPI) specification of 400 pC/N.

Since the firing at 1285 °C for 90 minutes provided the best hysteresis loops and the highest piezoelectric coefficients among the conditions tested, it was chosen for firing the spheres. The complete firing schedule can be seen in Figure 2.4.

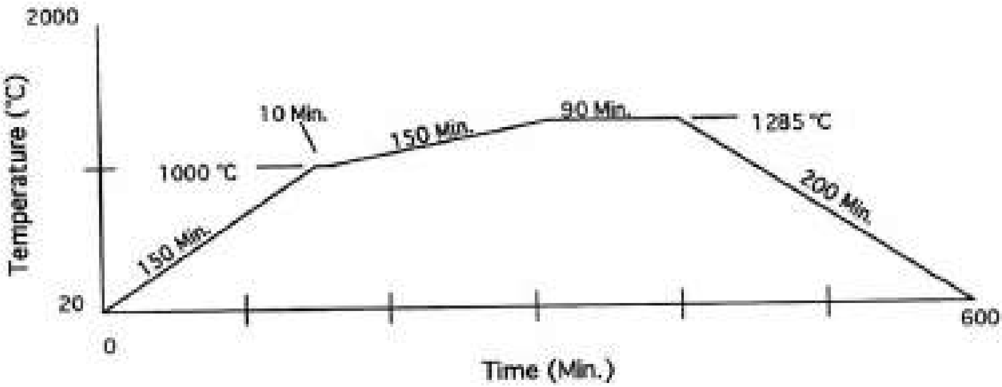

Figure 2.4

Firing Schedule for PZT Disks

2.3 STATISTICAL SPHERE EVALUATION

One of the main objectives of this study is to evaluate the feasibility of producing PZT hollow sphere transducers by the Torobin method in large quantities at a reasonable fabrication cost. A major factor which must be considered is the reproducibility of the hollow spheres. Many of the most important specifications of the spherical transducers are dependent on their size, shape, and wall thickness. Properties such as the capacitance, piezoelectric constants, resonant frequencies, and the resonant peak sharpness are important when evaluating the performance of a transducer. Many of these factors also depend on the dimensions of the spheres and their uniformity. For complete evaluation, several groups of spheres were taken through the different steps of fabrication, from receiving through completion, to quantify the yield data which can be expected. These data would not only provide information on which production steps should be addressed for improvement, but also help suggest improvements in future processing methods.

Many of the spheres have catastrophic flaws when they arrive. A high percentage of the spheres have small cracks, small holes, or even large flaws. Some of the spheres were malformed in the initial forming process and some were damaged during shipping due to the delicate nature of the green spheres. An initial flaw test is developed to screen out imperfect spheres before proceeding through the remaining fabrication steps. The test is called the "sink-float test" and is described in section 3.1.2.

After the initial flaw test, a lot of 100 spheres was selected to be tracked and evaluated through each of the processing steps. The sphere dimensions, weight, effective density, and aspherodicity were evaluated in the green state. Weight loss during burnout and sintering steps were monitored. Then, after firing, these same parameters were again measured. The spheres were then mounted and lapped down to hemispheres so the wall thickness could be measured with a Model ES-30 Environmental Scanning Electron Microscope (Electro Scan).

2.4 TRANSDUCER PREPARATION

2.4.1 Introduction

One of the objectives of this study was to design a fabrication procedure which would facilitate the mass production of tiny hollow sphere PZT transducers. To accomplish this, each procedure in the fabrication process was addressed and evaluated separately in search of improvements. This section describes the optimum method found for each step in the procedure, and discusses the steps taken to reach that designation.

2.4.2 Firing Procedure

(a) Burnout Stage

The purpose of the burnout stage is to expel any remaining solvent residue and to remove all of the organic binder added to the slurry to aid in shape retention of the spheres during the forming and drying procedures. TGA analysis was used to monitor weight loss of the PZT spheres when heated. A scanning rate of 10° C/min. was used for the experiment. From the results (Figure 2.5) it can be seen that the binder and residue is almost completely burned out at a temperature of 370 °C. Therefore, a burnout stage of 550 °C for 30 minutes in air at atmospheric pressure was chosen. 550 °C was chosen because it is sufficiently high to be sure all of the byproducts of the binder are driven out of the spheres, but low enough to insure minimal loss of lead at the sphere surface (Holman and Fulrath, 1973). The burnout schedule is shown graphically in Figure 2.6.

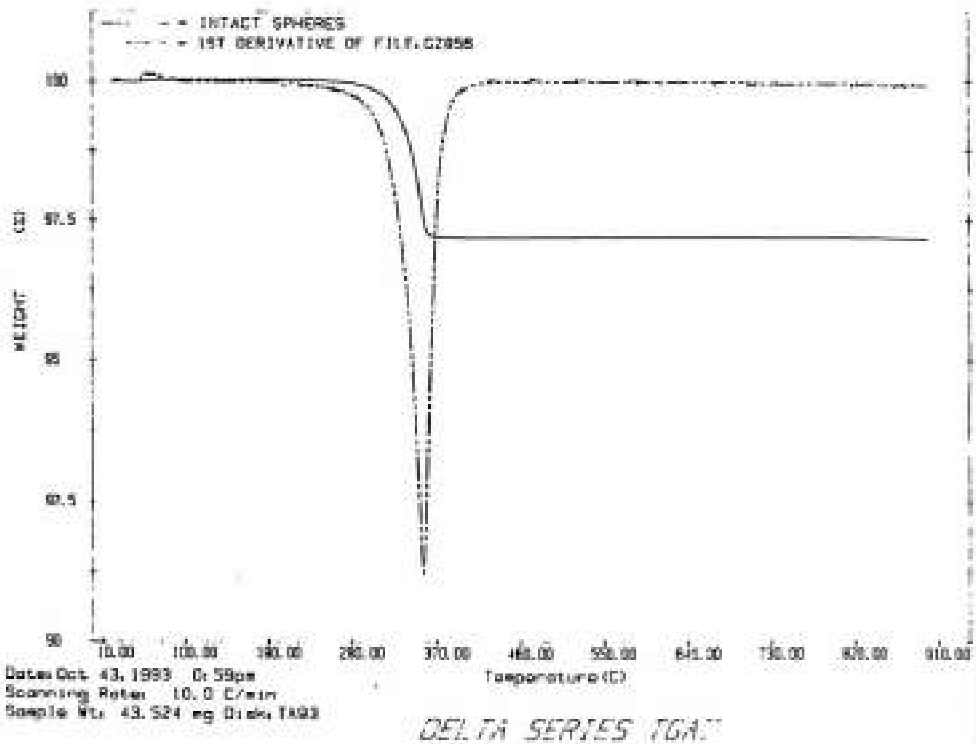

Figure 2.5

Graph of the TGA Analysis

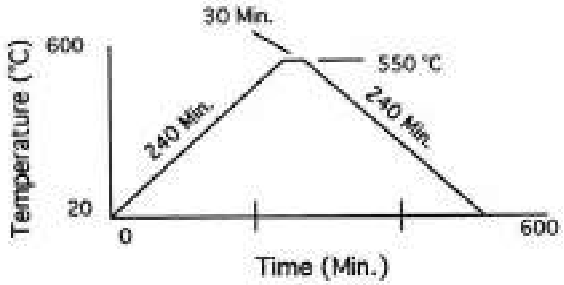

Figure 2.6

Burnout Schedule for PZT Spheres

(b) Sintering

The sintering procedure for the spheres was chosen on the basis of the time - temperature matrix study on the PZT pellets. It was shown in section 2.2.3 that a sintering temperature of 1285 °C for a time of 90 minutes in a lead rich atmosphere produced optimal values from the pellets with respect to dielectric and piezoelectric measurements (Figure 2.4). Thus this schedule was chosen for the PZT hollow spheres. The lead source was provided by including an alumina boat with 1.5 grams of mixed powder (18 parts PbO to 10 parts ZrO_2, by weight) in the crucible during sintering.

2.4.3 Drilling

In order for the spheres to be electroded on the inner surface a small hole had to be made through the thin wall. An initial attempt was made to drill the spheres by placing them in a fixture and drilling them using a drill press with a #60 (1.016 mm) bit. Due to the point loading created by the sharpened bit the majority of the spheres cracked. It was found that this problem could be alleviated by mounting the spheres in Crystal Bond 509 (Aremco Products, Inc.), which has a low melting point (135 °C) and can be readily dissolved in acetone.

Several spheres were placed into a circular mold and liquid Crystal Bond was poured in, completely submersing them. After the Crystal Bond cooled and solidified, the plug was removed from the fixture. This allowed the spheres to be drilled without cracking at a very high rate of approximately 10 spheres / minute. Once the spheres were drilled, the plug was reheated above the melting temperature of the polymer and the spheres were removed. Residue remaining on the spheres was removed in acetone. A typical plug can be seen in Figure 2.7.

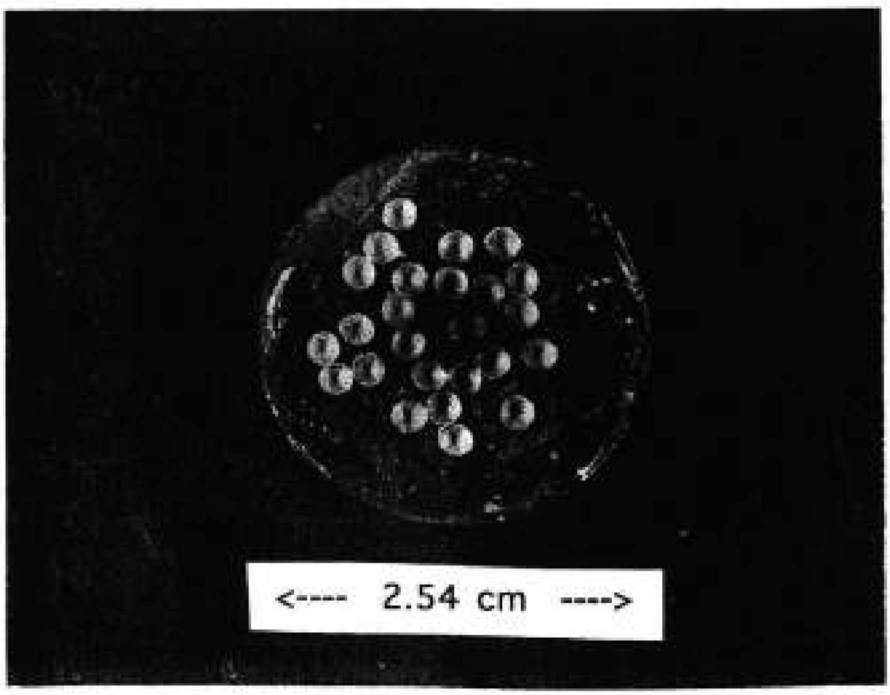

Figure 2.7

Typical Plug used for Drilling

2.4.4 Electroding

(a) Inner Surface

One of the most difficult steps of the fabrication procedure is achieving a uniform inner electrode with good integrity. Several different options for completing this were studied to decide on the best way to apply the inner electrode.

The optimum method for electroding the inner surface was to mount and drill the spheres, remove them from the plug, wash off any residue, and then electrode each sphere separately. This permitted the sphere to be held at an angle which allowed the air to escape when the electrode was injected (Figure 2.8). The electrode material used was an air dry silver paint solution called Conductive Silver 200 (Demetron, Inc.). Each sphere was completely filled with the electrode solution. The electrode was then dried for several hours. Although this method is labor intensive and time consuming, it produced the best dielectric and piezoelectric properties for the spheres.

When transferred to mass production, an air powered potting machine could be utilized to carefully meter the amount of injected electrode material into several spheres at the same time when placed onto a fixture. This would increase the efficiency of this step markedly.

Less successful results were obtained when air was trapped in the sphere during electrode injection. The resulting unelectroded surface within the sphere degraded the subsequent dielectric and piezoelectric properties of the sphere.

(b) Insulation Gap

Prior to applying the outer surface electrode, the drilled hole and a narrow insulation band were covered with a thin layer of rubber cement as shown in Figure 2.9. The insulation band insured there would be no shorting between the inner and outer electrodes. Once the outer electrode was applied, the rubber cement could be removed easily with a pair of tweezers. This procedure provided a clean insulation band around the hole.

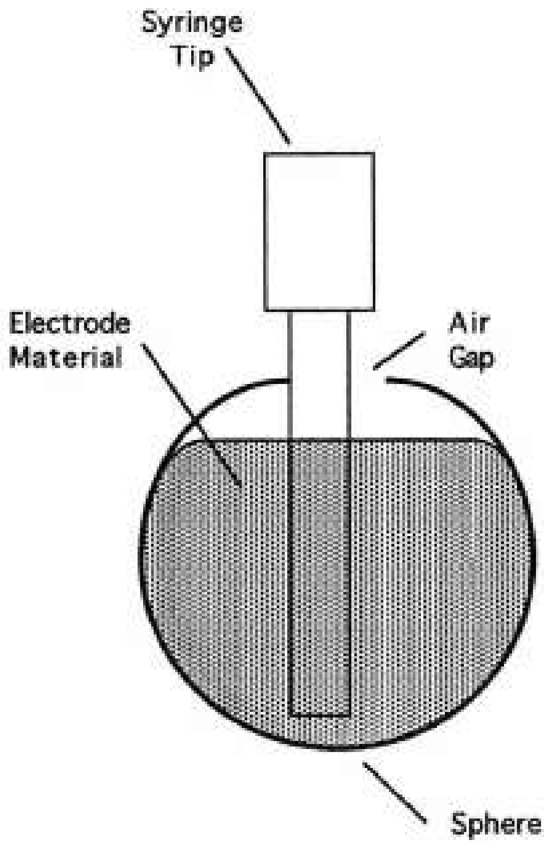

Figure 2.8

Electroding Procedure Showing Air Gap

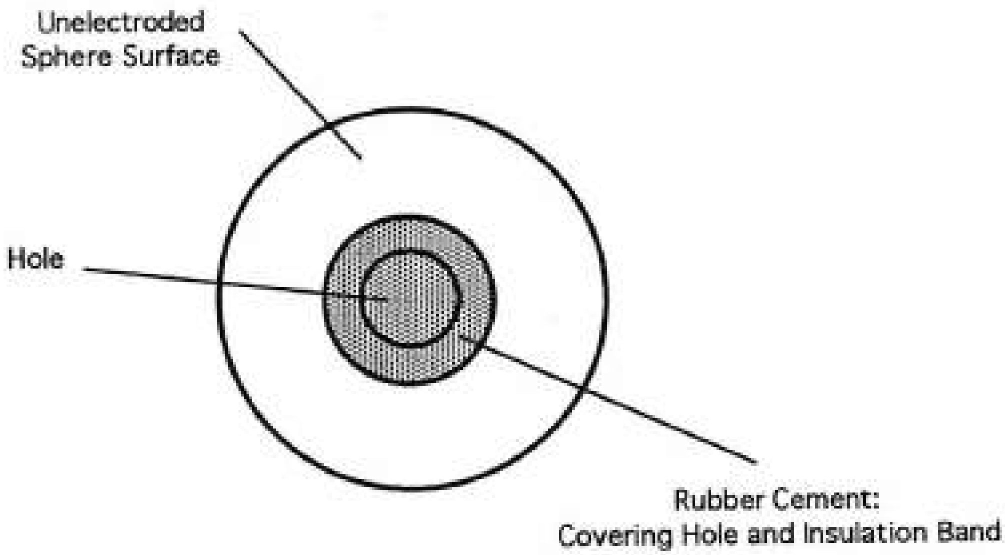

Figure 2.9

Sphere with Rubber Cement Covering

the Insulation Band

(c) Outer Surface

The best outer electrodes were obtained by placing the spheres in a fixture (Figure 2.10) and sputter coating them with gold for one minute. The process was then repeated on the other side to provide an even electrode coat over the sphere surface.

An initial attempt was made to achieve an outer electrode by painting the air dry Conductive Silver 200 on the exterior surface of the sphere with a paint brush. Upon drying, however, areas of poor electrode continuity were observed due to the high percentage of volatile vehicle (~75%) in the electrode material.

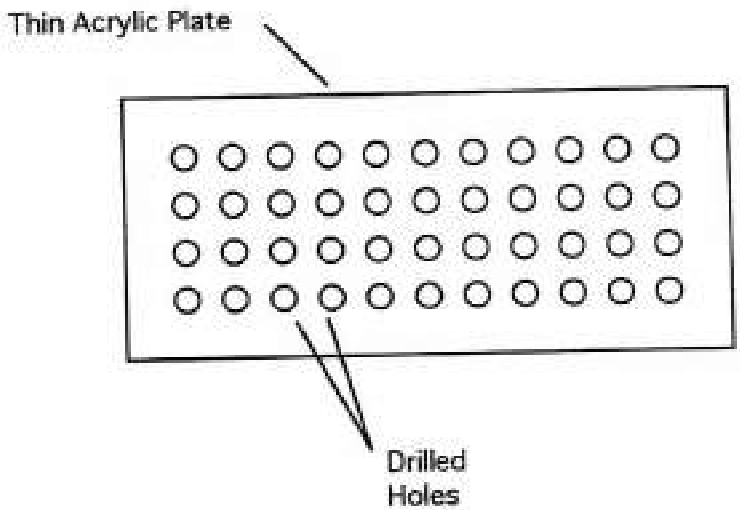

Figure 2.10

Fixture for Sputtering the Outer Electrode

2.4.5 Electrical Lead Wires

Silver lead wires (76.2 μm in diameter) were attached to the inner and outer electrodes using Epo Tek conducting silver epoxy (Epoxy Technology, Inc.). The epoxy was cured at 250 °C for 1 hour. Small "feet" (Figure 2.11) were made at the connecting ends of the lead wires to insure a good connection.

Figure 2.11

Feet at the Connecting Ends

of the Lead Wires

2.4.6 Sealing

Closing of the holes in the drilled spheres is accomplished by covering the hole with Ecobond 45 Epoxy (Emerson Cumming) and allowing it to cure. The spheres are then sealed by dip coating them into Hysol Casting System us-0089 (Dexter Electronic Materials Division), a two part chemically-reacted polyurethane coating. The function of the covering and sealant is to trap air inside the sphere and to permit the hydrostatic and water tank testing procedures where the spheres are submerged in liquid. Closing the drilled hole with a stiff, strong epoxy also aids in recovering the loss in strength caused by the hole, as the sealed spheres withstand a pressure of over 180 MPa during the hydrostatic testing without cracking or leaking.

2.5 CHARACTERIZATION OF PZT HOLLOW SPHERE TRANSDUCERS

Characterization was carried out on the PZT hollow sphere transducers to evaluate their potential for use in biomedical applications and hydrophone applications. Dielectric and piezoelectric measurements are reported. Admittance and phase versus frequency plots were obtained using an HP 4194A Impedance / Gain - Phase Amplifier to observe the resonant frequency and peak sharpness of both the low frequency breathing mode and the high frequency wall thickness mode characteristic of spherical shells. Hydrostatic measurements were carried out to give values of d_h coefficients for comparison with other hydrophone materials and composites. Finally, ultrasonic impulse response measurements were taken on the spheres to evaluate their usefulness as pulse-echo transducers in liquid mediums.

CHAPTER 3

RESULTS AND DISCUSSION

3.1 STATISTICAL SPHERE EVALUATION

3.1.1 Introduction

The response and resonant frequency of a piezoelectric transducer is directly related to its mass, size, and shape. Due to the extremely thin walls of the PZT hollow spheres in this investigation, uniformity of the diameter and wall thickness is of utmost importance when evaluating the repeatability of the spheres' properties for use as an omnidirectional transducer. The following section describes the sphere evaluation carried out in this study on unsintered and sintered spheres.

3.1.2 Sink - Float Test

A method to determine and remove any damaged spheres, coined the "Sink - Float Test", was designed to eliminate imperfect spheres in the green state before they were carried through the rest of the fabrication procedure. This test proved to be very useful, as many of the spheres possess defects which are undetectable to the naked eye. A description of the test follows.

The sink - float test experimental setup consists of a Pyrex beaker, a plunger, de-ionized water, and a vacuum chamber (Figure 3.1) .

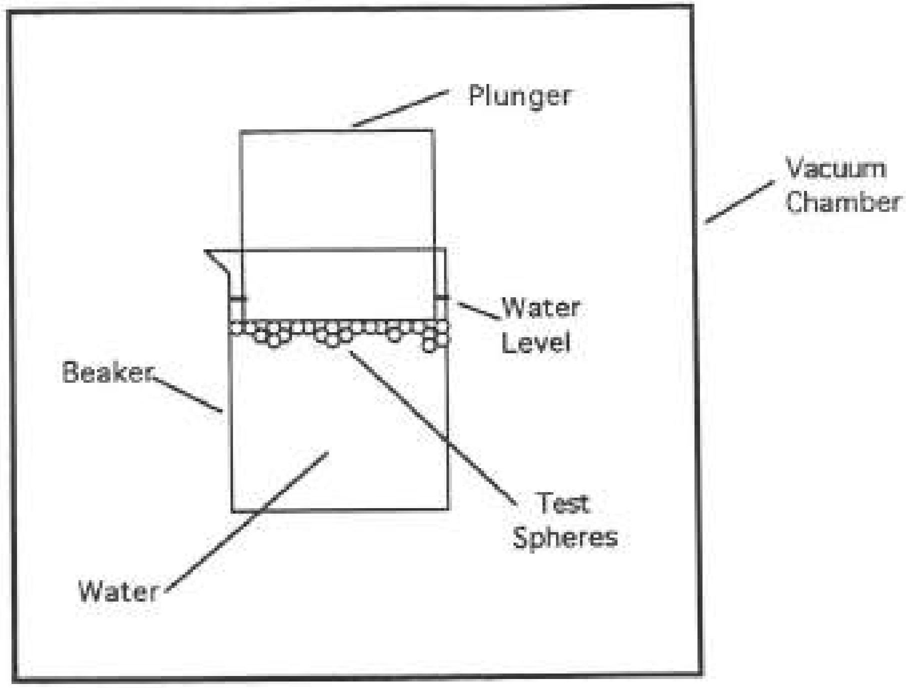

Figure 3.1

The Sink - Float Test Experimental Setup

The spheres to be tested are placed into the beaker. Water (de ionized) is then added. At this point nearly all of the spheres float due to their low green density of 0.65 - 0.8 g/cm^3. The only spheres which sink at this stage are the ones with flaws large enough to draw water into the central cavity of the sphere.

The plunger is then pushed down until the spheres are below the surface of the water. The beaker/plunger setup is then placed into a vacuum chamber where a vacuum of approximately 635 Torr is drawn and held for one minute before the chamber is allowed to return to atmospheric pressure (30 - 60 seconds).

As the vacuum is drawn on the beaker/plunger setup, small air bubbles can be observed escaping from the interior of damaged spheres. At this point, the flawless spheres still have air trapped inside, while the flawed spheres have a vacuum inside as a result of the escaped air. As the vacuum is released, water is drawn inside the cracked spheres, and they drop to the bottom of the beaker. The floating spheres are skimmed from the top to go on to the remaining steps in the fabrication procedure.

Approximately 50% of the green spheres in the as-received condition had visible flaws such as small and large holes, dimples, and cracks. These could be visually screened as unacceptable.

Only 20% of the as-received spheres passed the sink float test. That means that 30% more spheres failed the test than had been visibly screened. Consequently, it was determined that many of the spheres possess flaws which are small enough not to be observed through the visual inspection separation procedure mentioned above. It is for this reason that the sink-float test proved to be necessary and valuable.

For this investigation 100 spheres which had passed the sink-float test were selected for tracking throughout the firing procedures. Statistics were taken on the outer diameter, wall thickness, shrinkage, weight loss, and deformation during sintering.

3.1.3 Green Sphere Evaluation

The first step was to weigh each of the spheres on a four digit Metler AE200 scale. A histogram of the results is shown in Figure 3.2. The average weight of the green spheres was 14.2 mg ± 0.44 mg.

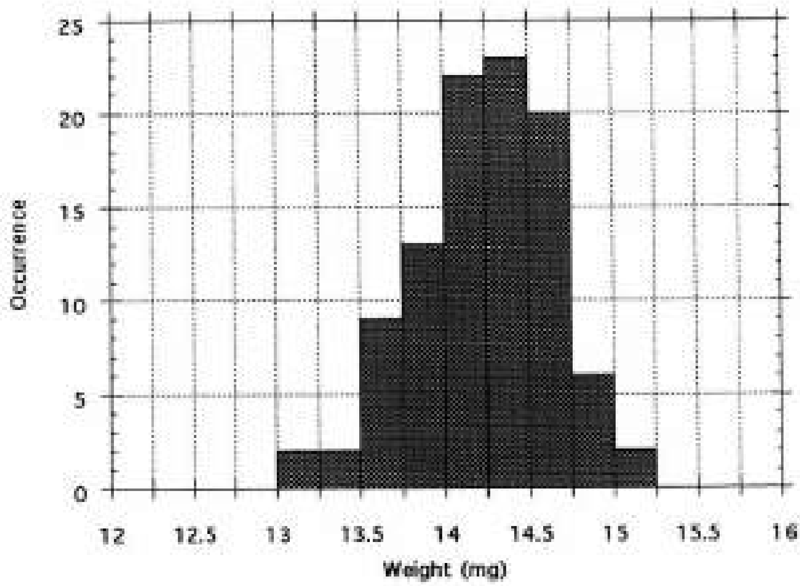

Figure 3.2

Weight Distribution of the Green Spheres

Next, the outer diameter of each sphere was measured in two perpendicular directions using an optical comparator. From this data, an average outer diameter of each green sphere was calculated and plotted (Figure 3.3). The average outside diameter for the spheres is 3.31 mm ± 0.037 mm.

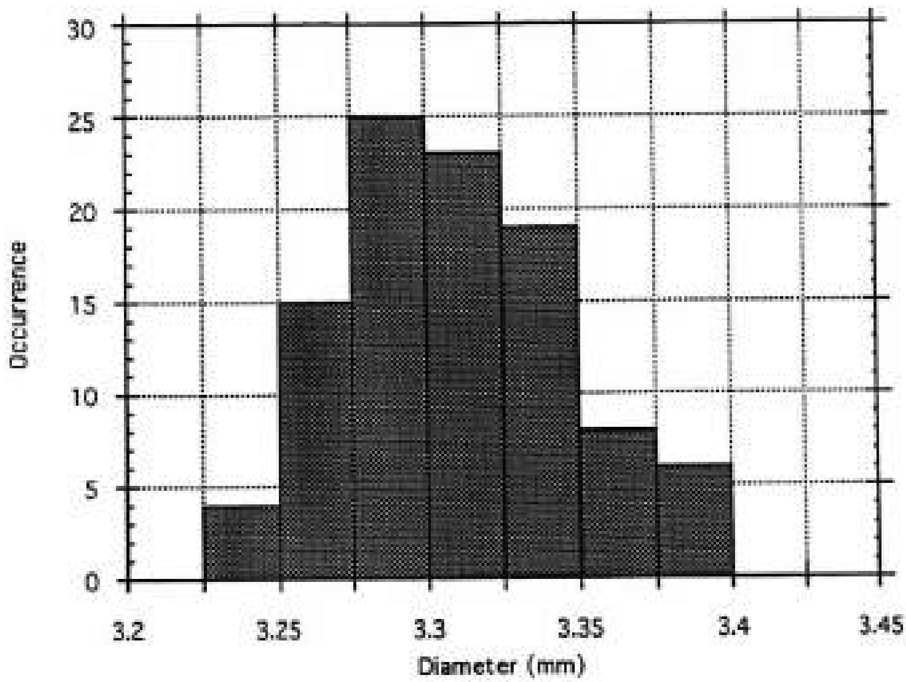

Figure 3.3

Average Outside Diameter Distribution of the Green Spheres

Since the diameter measurement was taken with the largest diameter in the x direction, the % aspherodicity is calculated by:

$$\frac{dia.x - dia.y}{ave.dia.}(100) = Aspherodicity(\%) \qquad \text{Equation 3.1}$$

The average aspherodicity of the 100 green spheres was calculated to be 1.88%, with a maximum of 6%.

3.1.4 Sintered Sphere Evaluation

The first step of the sintered sphere evaluation was to weigh the mass of each fired sphere to four significant figures (See Figure 3.4). The average weight of the sintered spheres was 13.8 mg ± 0.43 mg.

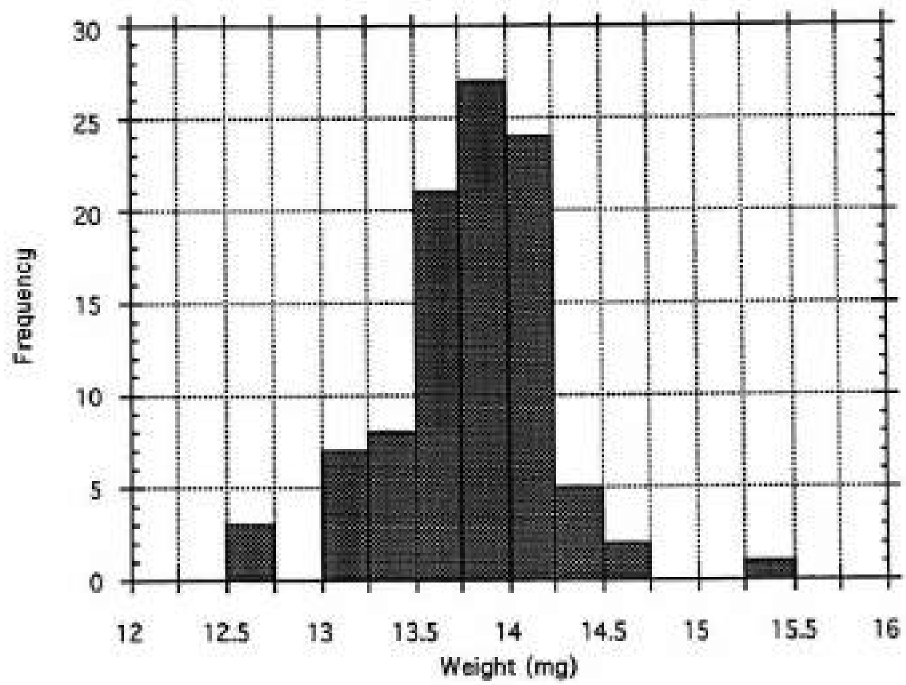

Figure 3.4

Weight Distribution of the Sintered Spheres

Next, the outer diameter of each sphere was again measured in the x and y direction. From this data, the average outer diameter of the sintered spheres was calculated (See Figure 3.5). The average outside diameter of all of the sintered spheres is 2.76 mm ± 0.039 mm. The shrinkage is 16.6%, which is typical of the amount of volumetric shrinkage noted in standard PZT processing. The average aspherodicity of the sintered spheres is 2.28%, with a maximum of 8.1%.

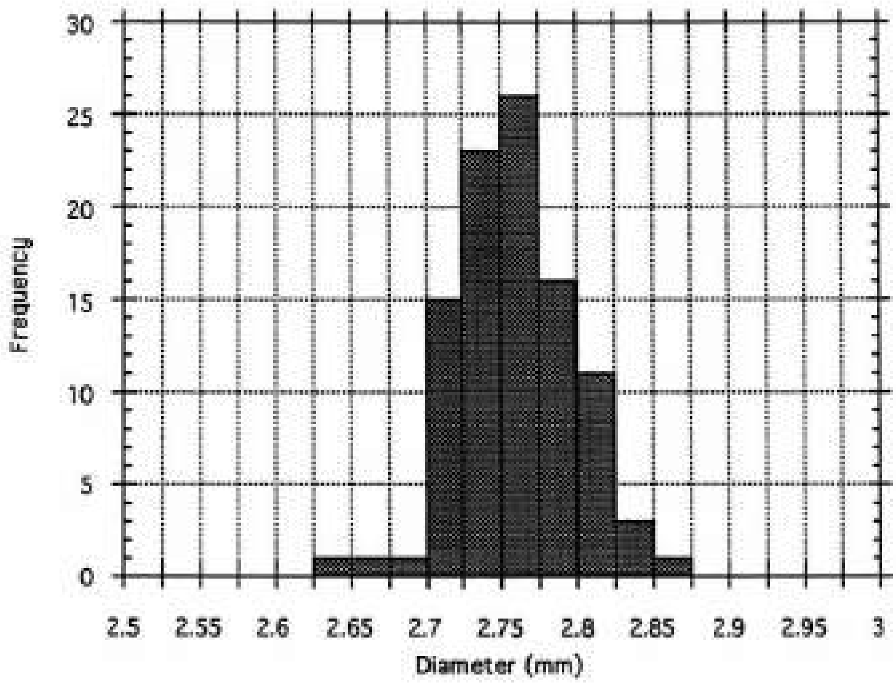

Figure 3.5

Outer Diameter Distribution of the Sintered Spheres

Since the weight and the average diameter of each of the sintered spheres is known, the approximate inner radius of the inside wall is calculated using the following equation:

$$r_i = \sqrt[3]{r_o^2 - \frac{3}{4\pi}\left(\frac{m}{\rho}\right)}$$

Equation 3.2

where r_i = the inside radius, r_o = the outside radius, m = the mass of the individual sphere in mg, and ρ = the density of PZT (UPI 501A powder = 7.7 g/cm^3). The results are plotted in a histogram in Figure 3.6. The average inside radius of all of the sintered spheres is 1.30 mm ± 0.022 mm.

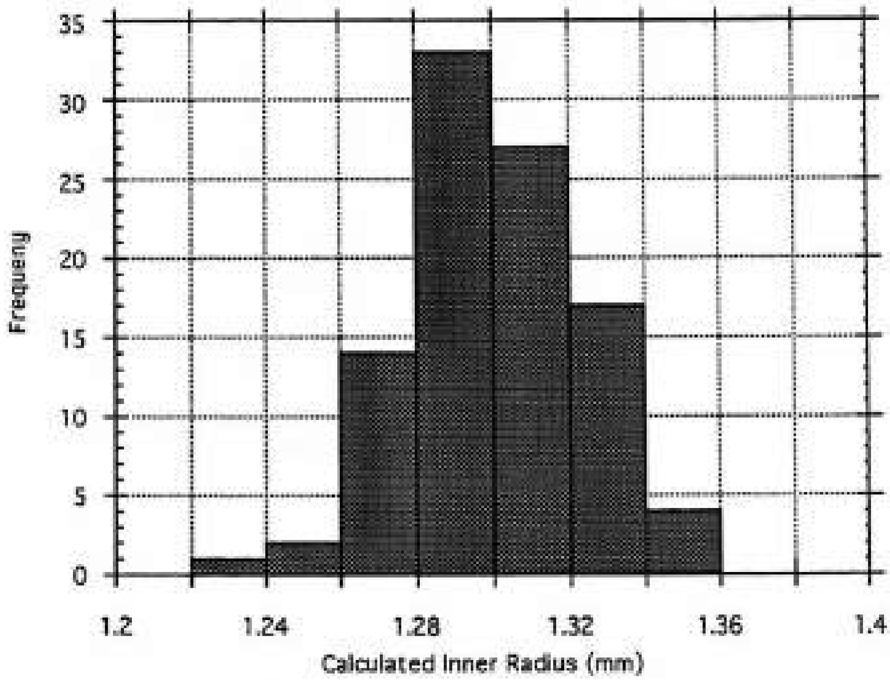

Figure 3.6

Calculated Inner Radius Distribution for Sintered Spheres

With the inner and outer diameters known for each individual sphere, the wall thickness is calculated by:

$$r_o - r_i = Wall\_Thickness \qquad \text{Equation 3.3}$$

The results are shown in Figure 3.7. The average sintered wall thickness is 79.4 μm ± 0.37 μm.

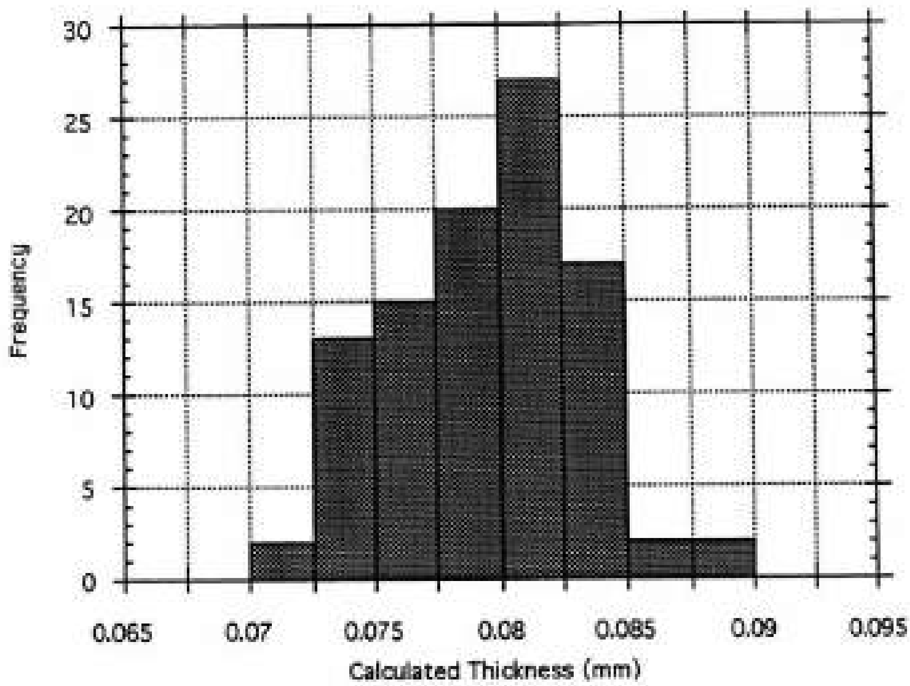

Figure 3.7

Calculated Average Wall Thickness Distribution

for Sintered Spheres

The effective density of the spheres, including the trapped air, is calculated from Equation 3.5, since the mass and the outside diameter of each individual sphere is known.

$$\rho_{eff.} = \frac{m}{\frac{4}{3} r_o^3 \pi}$$

Equation 3.4

A graph of the density data is shown in Figure 3.8. The average density of the PZT sintered spheres is 1.25 g/cc ± 0.068 g/cc.

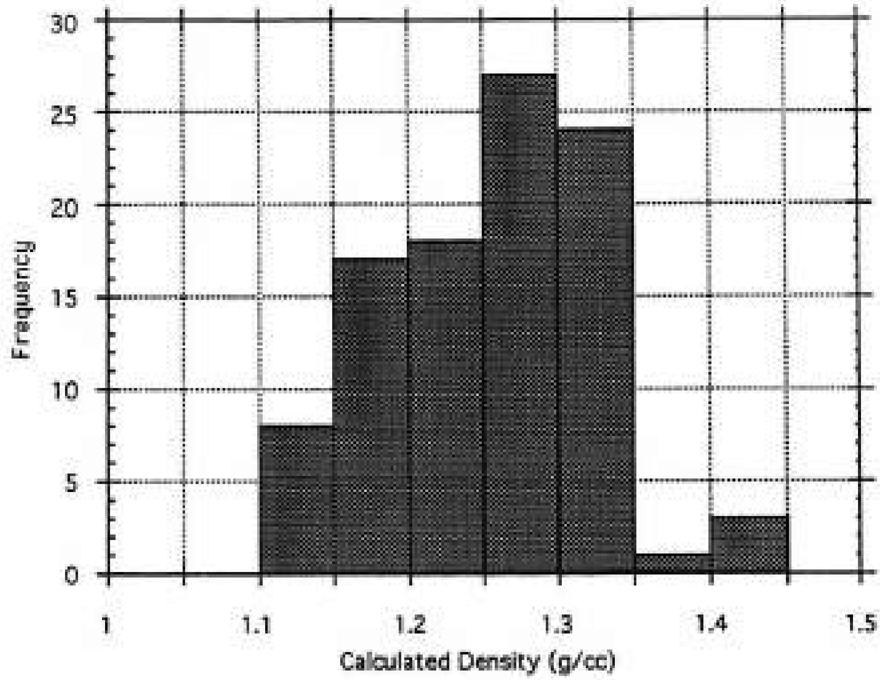

Figure 3.8

Distribution of the Effective Density for Sintered Spheres

3.1.5 Weight Loss

Due to the delicate nature of the spheres in the burned out state, the weight loss measurements during burnout and sintering were taken on all of the spheres simultaneously while in the platinum sintering tray.

The spheres were placed into the platinum tray in the green state and weighed to four decimal point accuracy. Following burnout, the spheres were weighed again. From this data, the calculated weight loss after burnout but before sintering is 3.1%. This corresponds to the 3-3.5% binder usually added in PZT ceramic processing to aid in shape retention.

The spheres were then sintered and the final weight was measured. No detectable weight loss was measured as a result of Pb loss during sintering.

3.1.6 Sphere Wall Thickness Variation

Initial results from the statistical sphere evaluation suggest that the wall thickness of the spheres is approximately 80 μm ± 10%. However, this data is the average wall thickness of the spheres. It reveals no information of the variation in the wall thickness within each individual sphere. Weak and broad wall thickness peaks in the admittance spectra (Section 3.2.4) suggest that the variance in wall thickness within each individual sphere is considerable. Therefore, the wall thickness variation was investigated using electron microscopy.

Twenty five sintered spheres were mounted in Epo Kwick (Buehler) and allowed to cure for 1 hour. The plug was then cut in half through the diameter with a diamond saw, exposing the hemisphere cross section of the spheres. The plug was then polished using 0.5 μm diamond paste. An environmental scanning electron microscope (ESEM) was then used to measure the wall thickness at several positions around each sphere. The wall thickness variation within each sphere was large. Typically, the thick to thin areas of the walls varied by a ratio of 3 to 1. That is, for a sphere with an area of large wall thickness of 80 μm, there is an adjacent thin wall area of about 25 - 30 μm. The sphere manufacturer has also found in independent studies that the fabrication procedure used often leads to spheres with a thick stripe in the center and two thinner endcaps, and that a 3 to 1 ratio in the wall thickness is common. Improvements in the sphere fabrication procedure are under investigation to alleviate this problem. Pictures showing the wall thickness variation at different points on a typical sphere are shown in Figures 3.9.

(a)

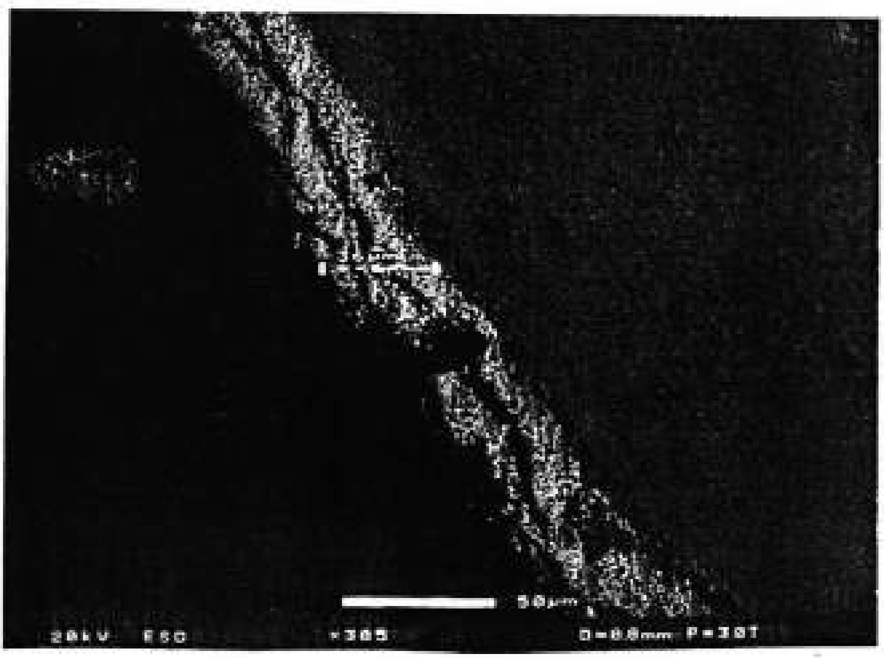

(b)

Figure 3.9

Wall Thickness Variation for a Typical Sphere

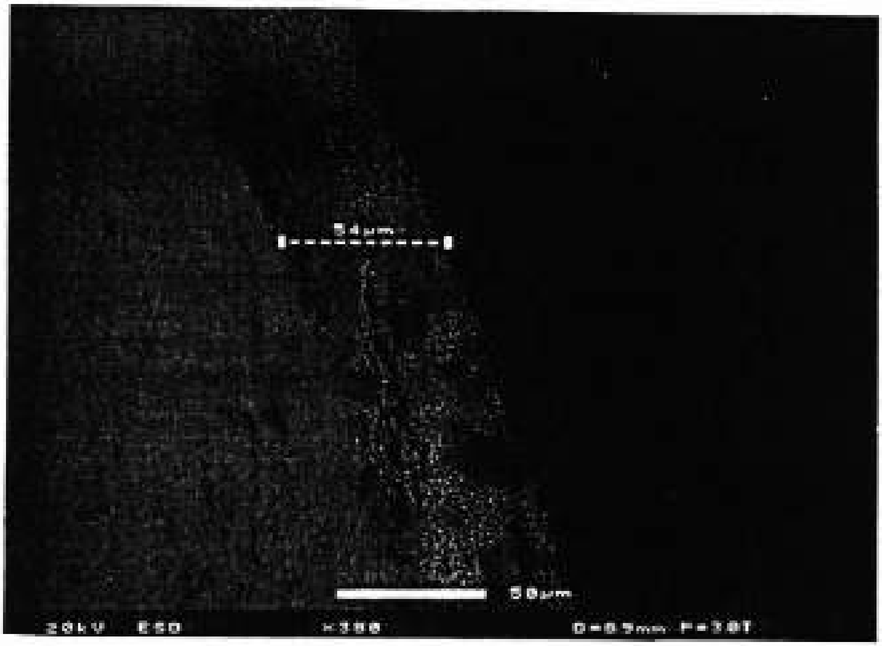

c)

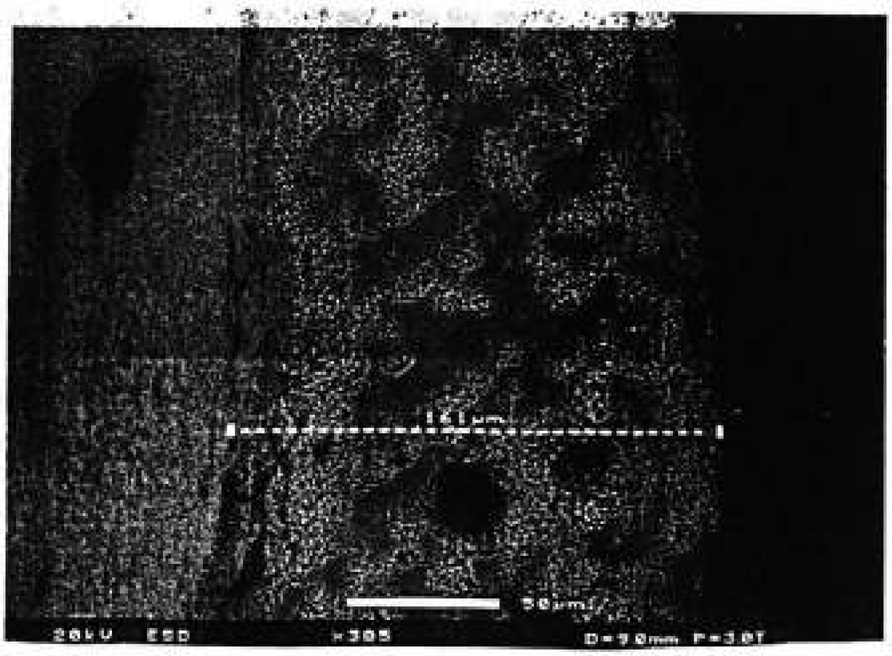

(d)

Figure 3.9 (continued)

Wall Thickness Variation for a Typical Sphere

The ESEM micrographs also revealed defects within the thin sphere walls. In all of the spheres many cracks and large pores were observed, along with areas of poor density. Examples of these defects are shown in Figures 3.10 and 3.11, respectively.

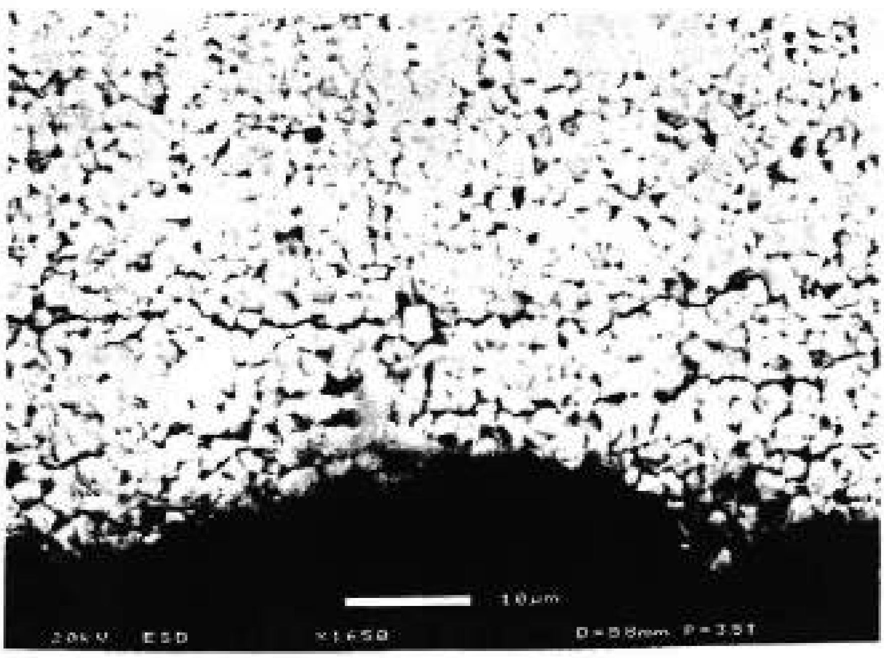

Figure 3.10

Cracks Observed in the Sphere Walls

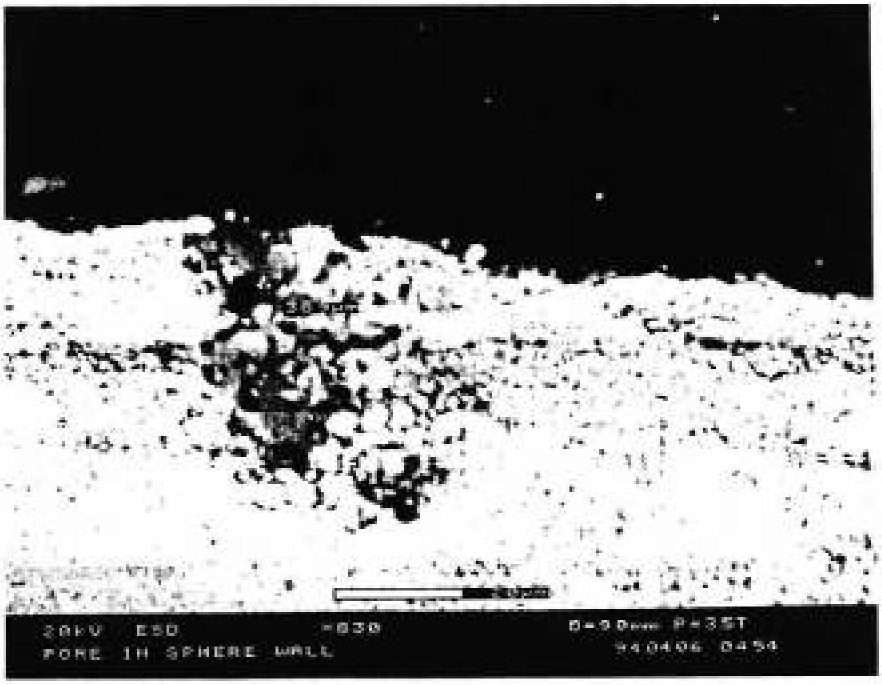

Figure 3.11

Porosity Observed in the Sphere Walls

3.2 CHARACTERIZATION OF PZT SPHERICAL TRANSDUCERS

3.2.1 Introduction

In order to evaluate the spherical transducers' potential for use as hydrophones or in biomedical applications, several properties of the PZT spheres were measured and compared to other standard materials and transducer designs. The properties evaluated were the dielectric constant and loss, the resonance spectra, the coupling coefficients, hydrostatic piezoelectric measurements, and the submerged impulse response of the spheres. The experimental setup and data for each of the tests is presented and discussed subsequently.

Due to continual improvements in the fabrication procedure, the characterization described in this section will focus on the final batch of ten spherical transducers produced. This batch significantly outperformed the previous batches.

3.2.2 Dielectric Measurements

Low frequency dielectric measurements for poled spheres were obtained using an HP 4274A Multi-Frequency LCR Meter at a frequency of 10 KHz and a driving voltage of 0.1 volt. A list of the values measured is provided in Table 3.1. The average capacitance of the PZT spheres is 1438 pF and the average dielectric loss factor (tan d) is 0.0365. The variance in the data is attributed to the inconsistent wall thickness between samples, as described in the statistical sphere evaluation.

The approximate dielectric constant (K) of each of the spheres can be calculated from Equation 1.3, using the measured capacitance and data for the area and thickness from the statistical sphere evaluation undertaken in this investigation (Section 3.1). The values for the dielectric constants calculated are provided in Table 3.2. The average dielectric constant for the spheres is 675. The value of K for the spheres is significantly lower than the value of 1720 measured for bulk PZT 501A from the same batch of initial powder (Section 2.2.3). The reason for this discrepancy is likely to be a combination of an imperfect inner electrode and the low density and porosity observed in the sphere walls in Section 3.1.6. The variance in the dielectric constant between spheres may be a result of using an average area and wall thickness in the equation, as opposed to a true variation in material properties.

Table 3.1

Capacitance and Loss Measurements on PZT Spheres

at 10 KHz and 0.1 Volt

Sphere #	Cap. (pF)	Loss (tanδ)	Sphere #	Cap. (pF)	Loss (tanδ)
1	1127	0.033	6	1505	0.034
2	1842	0.038	7	1168	0.035
3	1885	0.036	8	1074	0.036
4	1616	0.043	9	1496	0.038
5	1469	0.037	10	1020	0.035

Table 3.2

Calculated Dielectric Constant (K) of the PZT Spheres

Sphere #	K	Sphere #	K
1	531	6	709
2	867	7	550
3	887	8	506
4	761	9	704
5	692	10	480

3.2.3 Piezoelectric Measurements

(a) Hysteresis (P-E) Loops

Hysteresis loops were obtained on the spheres using the system described in Section 2.2.3(b). A schematic of the setup is shown in Figure 2.2. Since a large voltage is applied to the spheres when acquiring the data for a hysteresis loop, this test takes the place of the poling step usually carried out to align the domains in a bulk sample. A typical hysteresis loop from a PZT spherical transducer is shown in Figure 3.12.

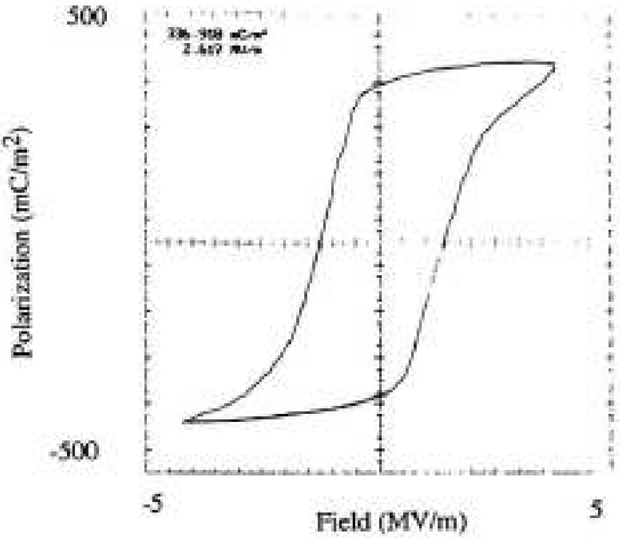

Figure 3.12

Typical Hysteresis Loop from a PZT Spherical Transducer

Values for the remanent polarization (P_r) and coercive field (E_c) of each sphere were taken from the hysteresis loops and are displayed in Table 3.3. The average remanent polarization and coercive field of the PZT spheres are 319 mC/m^2 and 2.1 MV/m, respectively.

Table 3.3

Remanent Polarization(P_r) and Coercive Field(E_c)

of PZT Spherical Transducers

Sphere #	P_r(mC/m^2)	E_c(MV/m)	Sphere #	P_r(mC/m^2)	E_c(MV/m)
1	224	1.9	6	322	1.8
2	352	1.9	7	299	2.3
3	358	1.9	8	262	2.3
4	348	2.6	9	368	2.5
5	343	2.3	10	275	2.3

(b) Hydrostatic (d_h) Measurements

Hydrostatic d_h measurements were taken on the spherical transducers for comparison with other hydrophone materials and composites. A schematic of the experimental setup is shown in Figure 3.13.

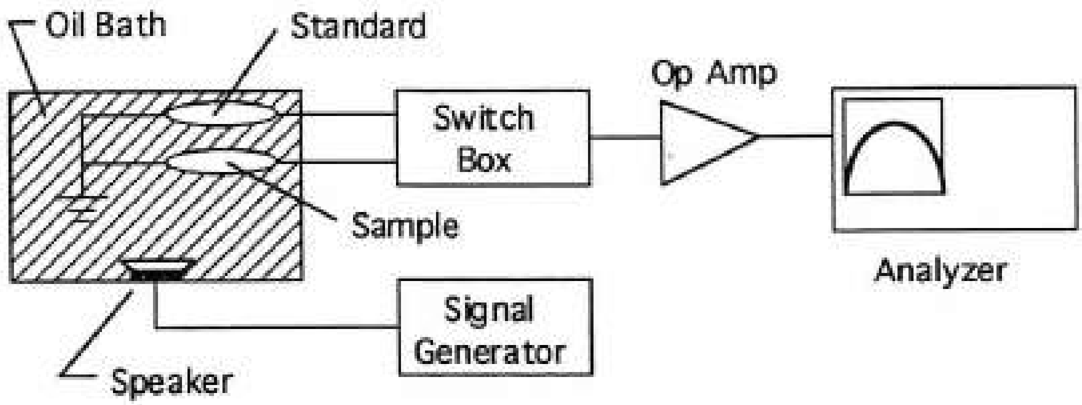

Figure 3.13

Schematic of the d_h Measurement Experimental Setup

The hydrostatic piezoelectric coefficient d_h is defined as the ability of an appropriate sensor to produce electrical charge when subjected to a pressure in all directions simultaneously. In the experiment the oil acts as a sonic medium for the wave output from a speaker, generated by a signal generator. A frequency of 40 Hz was used for this experiment. The standard and the sample are placed into the oil bath and connected to a switch box for measurement selection. The charge generated by the sample or standard is converted to a voltage by the operational amplifier. This voltage is sent to an analyzer where the amplitude of the voltage is measured. Since the d_h of the standard is known, the d_h of the sample can be calculated by:

$$d_h = \frac{VA_s}{V_s A} d_{hs} \qquad \text{Equation 3.5}$$

where V = the measured voltage of the sample, V_s = the voltage measured from the standard, A_s = the area of the standard, A = the area of the sample, and d_{hs} = the d_h of the standard.

Measurements were taken on each sample by varying the pressure from 18.6 MPa to 186.0 MPa in 18.6 MPa increments, and recording the voltage of the standard and sample at 40 Hz. A graph of the values of d_h obtained for five samples is shown in Figure 3.14.

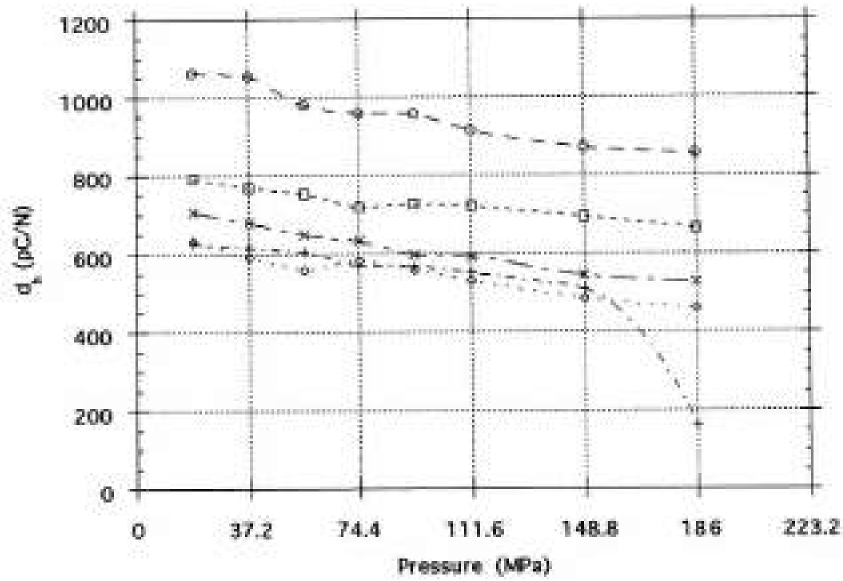

Figure 3.14

d_h Measurements on PZT Spheres

as a Function of Pressure

The d_h sensitivity of the spheres follow a trend of decreasing values as a function of increasing pressure. This is most likely due to deformation of the spheres under hydrostatic pressure. At lower pressures, deformation of the spheres due to the sound wave emanated by the speaker is largest, corresponding to the higher d_h values. At increasing pressures, the spheres can deform less , and the d_h values begin to shift downward accordingly.

As seen in the Figure 3.14, the d_h values obtained for the sealed PZT spheres are significantly higher than the d_h value expected for bulk PZT. The d_h values obtained for unsealed spheres coincided with d_h values for bulk PZT as expected, and were therefore not reported separately. The higher d_h values for the sealed spheres can be explained by evaluating the different stresses experienced by the sealed spheres. The two types of stresses observed are radial and tangential stresses (Timoshenko et al., 1951), which can be calculated by the following equations:

$$\sigma_R = \frac{P_o b^3(R^3 - a^3)}{R^3(a^3 - b^3)} - \frac{P_i a^3(b^3 - R^3)}{R^3(a^3 - b^3)}$$ Equation 3.6

$$\sigma_t = \frac{P_o b^3(2R^3 + a^3)}{2R^3(a^3 - b^3)} - \frac{P_i a^3(2R^3 + b^3)}{2R^3(a^3 - b^3)}$$ Equation 3.7

where R is the distance from the center of the sphere and the other variables are as depicted in Figure 3.15:

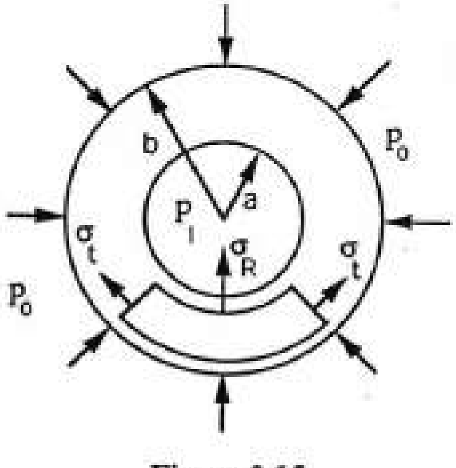

Figure 3.15

Description of Variables for the Sphere Model

First we considered the unsealed spheres where the pressure inside and outside the spheres is equal ($P_i = P_o$). The radial stresses on the inner and outer sphere walls can be calculated using known values for the inner and outer radii. At the outer surface, b = R and the equation can be reduced to:

$$\sigma_{r_o} = \frac{P_o b^3 \left(R^3 - a^3\right)}{R^3 \left(a^3 - b^3\right)}$$ Equation 3.8

therefore, the radial stress on the outer surface of the spheres under this condition can be calculated to be:

$$\sigma_{r_o} = -P_o$$ Equation 3.9

At the inner surface, a = R, and the equation can again be simplified to:

$$\sigma_{r_i} = \frac{P_o a^3 \left(b^3 - R^3\right)}{R^3 \left(a^3 - b^3\right)}$$ Equation 3.10

Again, substituting for a, b, and R yields:

$$\sigma_{r_i} = -P_o$$ Equation 3.11

The tangential stress can be calculated at the inner and outer surfaces. At the outer surface, where R = b, the stress can be calculated from:

$$\sigma_{r_o} = \frac{P_o 2b^3\left(b^3 - a^3\right)}{2b^3\left(a^3 - b^3\right)}$$ Equation 3.12

Substituting for a, b, and R yields:

$$\sigma_{r_o} = -P_o$$ Equation 3.13

at the inner surface, R = a, and the stress is:

$$\sigma_{r_o} = \frac{P_o 2a^3\left(b^3 - a^3\right)}{2a^3\left(a^3 - b^3\right)}$$ Equation 3.14

Again, substituting yields:

$$\sigma_{r_o} = -P_o$$ Equation 3.15

Therefore, for the unsealed spheres the stresses in the radial and tangential directions, at both the inner and outer surfaces, is equal to that of the applied pressure (P_O) and are negative denoting a compressive stress. Thus, a sphere with a hole can be thought of as an unwrapped sphere, where it can be treated as a typical bulk sample and all of the standard equations and constants apply. Hence, the expected d_h of the unsealed spheres can be calculated from the equation:

$$P_3 = d_{33}\sigma_3 + d_{31}\sigma_1 + d_{32}\sigma_2$$ Equation 3.16

substituting Po for $s_{1,\,2,\,\text{and}\,3}$, d_{33} = 400 pC/N, and $d_{33} = d_{31}$ = -175 pC/N gives:

$$P_3 = -P_o\left(50\,{}^{pC}\!/_{N}\right)$$

Equation 3.17

and since $P_3 = -P_o (d_h)$, d_h should be 50 pC/N for a perfect PZT oil filled sphere with optimum properties. The measured value in this study was ≈ 10 pC/N. The low d_h measurements for the unsealed PZT spheres is attributed to the deviations from a perfect shape, and the sphere wall density problems.

For the sealed spheres, where P_o = the outer pressure and P_i = the inner pressure = 0, the equation for the radial stress in the sphere reduces to:

$$\sigma_R = \frac{P_o b^3 \left(R^3 - a^3\right)}{R^3 \left(a^3 - b^3\right)}$$

Equation 3.18

at the outer surface where R = b, substituting gives:

$$\sigma_{r_o} = -P_o$$

Equation 3.19

and the inner surface where R = a, substituting gives:

$$\sigma_{r_i} = 0$$

Equation 3.20

Therefore, the average radial stress on the sphere wall is:

$$\sigma_{r_{ave}} = \frac{-P_o}{2}$$

Equation 3.21

Substituting Pi = 0 into the tangential stress equation yields:

$$\sigma_{\tau} = \frac{P_o b^3 \left(2R^3 + a^3\right)}{2R^3 \left(a^3 - b^3\right)}$$
Equation 3.22

simplifying and substituting R = b for the tangential stress at the outer surface gives:

$$\sigma_{\tau_o} = \frac{P_o b^3 \left(2b^3 + a^3\right)}{2\left(a^3 - b^3\right)}$$
Equation 3.23

substituting, a = 1.30 x 10^{-3} m and b = 1.38 x 10^{-3} m:

$$\sigma_{\tau_o} = -8.64 P_o$$
Equation 3.24

For the tangential stress at the inner surface where R = a, the equation simplifies to:

$$\sigma_{\tau_i} = \frac{P_o\left(3b^3\right)}{2\left(a^3 - b^3\right)}$$
Equation 3.25

and substituting gives:

$$\sigma_{\tau_i} = -9.14 P_o$$
Equation 3.26

Therefore, the effective tangential stress on the surface is:

$$\sigma_{\tau_{ave}} = \frac{-8.64 - 9.14}{2} P_o = -8.89 P_o$$
Equation 3.27

From this, it is clear that the spherical geometry of the transducer leads to a magnification of the incoming stress wave. Thus, the walls of the hollow PZT spheres used in this study experience a tangential stress nearly an order of magnitude higher than the stress due to the sound wave to be sensed. As a result, the sealed PZT spheres are much more sensitive to hydrostatic pressure waves than would be a PZT disk of the same area. This stress magnification is lost if the pressure on the inside of the sphere is equalized.

From these calculated stresses expected d_h values can be obtained for the sealed PZT spheres from:

$$P_3 = d_{33}\sigma_3 + d_{31}\sigma_1 + d_{32}\sigma_2$$ Equation 3.28

substituting the stresses gives:

$$P_3 = d_{33}\left(\frac{-P_o}{2}\right) + d_{31}(-8.89)P_o + d_{32}(-8.89)P_o$$ Equation 3.29

rearranging and substituting $d_{31} = d_{32}$:

$$P_3 = -P_o\left(\frac{d_{33}}{2} + 17.8d_{31}\right)$$ Equation 3.30

Since, $P_3 = -P_o\,(d_h)$, d_h is:

$$d_h = \frac{d_{33}}{2} + 17.8d_{31}$$ Equation 3.31

This accounts for the much larger d_h values exhibited by sealed spheres than by the oil-filled spheres. Filled spheres showed an average d_h of 10 pC/N, whereas, the sealed spheres shown in Figure 3.14 had values as high as ~1000 pC/N. When d_{33} = 400 pC/N and d_{31} = -175 pC/N, are substituted into equation 3.31, d_h is calculated to be -2915 pC/N for perfect sealed spheres with bulk piezoelectric properties. Consequently, as the properties of the PZT spheres are improved, d_h values as high as 3000 pC/N are expected to be achievable.

A ratio can be used to calculate the expected value of d_h for the sealed spheres used in this investigation. The calculated d_h of the spheres is 50 pC/N, the measured d_h for unsealed spheres is ~10 pC/N. Since, the calculated value of the d_h for the sealed spheres is 2915 pC/N, the approximate d_h measurements can be calculated by:

$$\frac{10}{50} = \frac{d_{h_{approx}}}{-2915\,{}^{pC}\!/_{N}} \qquad \text{Equation 3.32}$$

then:

$$d_{h_{expected}} = 585\,{}^{pC}\!/_{N} \qquad \text{Equation 3.33}$$

The average d_h measured for the sealed spheres was 676 pC/N. These numbers are comparable, suggesting that the models are appropriate.

3.2.4 Resonant Frequency

The ability of a transducer to operate effectively for a given application depends on the resonant frequency of the unit's characteristic modes of vibration. As described in

Section 1.4, a hollow sphere's primary mode of vibration is a breathing mode. The secondary vibration mode of a hollow sphere is a wall thickness mode. In this investigation both modes are equally important since the mode of vibration of interest depends on the particular application. Hydrophones depend primarily on the powerful breathing vibration mode to transmit and receive signals. It is expected that biomedical ultrasound transducers, which require better imaging resolution, will rely on the higher frequency thickness mode.

From the earlier investigation (Meyer, Jr. et al., 1994), the breathing mode resonance of the spheres has been calculated to be approximately 600 KHz, and the wall thickness resonance to be 14.5 MHz. Admittance and phase versus frequency plots have been obtained for each of the spherical transducers using an HP 4194A Impedance / Gain - Phase Amplifier. The resonant frequencies of the breathing and wall thickness modes are measured and shown in Table 3.4. A typical plot of the admittance and phase spectrum for a PZT spherical transducer, showing the breathing mode (a) and the thickness mode (b), can be seen in Figure 3.16.

Using the resonant / antiresonant frequency equation for the breathing mode resonance, the planar coupling coefficient (k_p) can be calculated by:

$$k_p^2 = \left(\frac{f_r^2}{f_a^2}\right) \quad \text{Equation 3.34}$$

The average coupling coefficient for the hollow spheres was calculated as 0.35. This value is smaller than the accepted value for bulk material (0.60). The reason for the lower value is probably due to imperfections in the spherical shape, and because the measurements were taken on spheres which were sealed with epoxy and coated with polyurethane. The epoxy and coating will cause the resonance peak to broaden, and thus cause a reduction in the measured planar coupling coefficient.

Table 3.4

Measured Resonant Frequency of the Breathing and Wall Thickness Modes of PZT Spherical Transducers

Sphere #	Breathing Mode Resonance (KHz)	Thickness Mode Resonance(MHz)	Sphere #	Breathing Mode Resonance (KHz)	Thickness Mode Resonance(MHz)
1	700	16.8	6	713	16.8
2	713	-	7	717	-
3	655	15.5	8	718	13.3
4	713	12.1	9	706	-
5	718	13.5	10	718	16.2

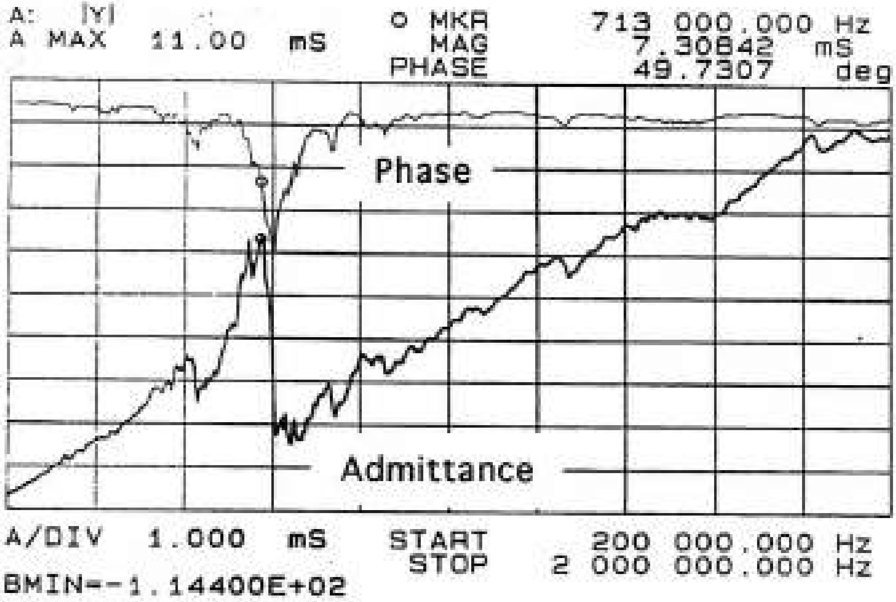

Figure 3.16(a)

Admittance and Phase Plot of a PZT Spherical Transducer

Showing the Breathing Mode

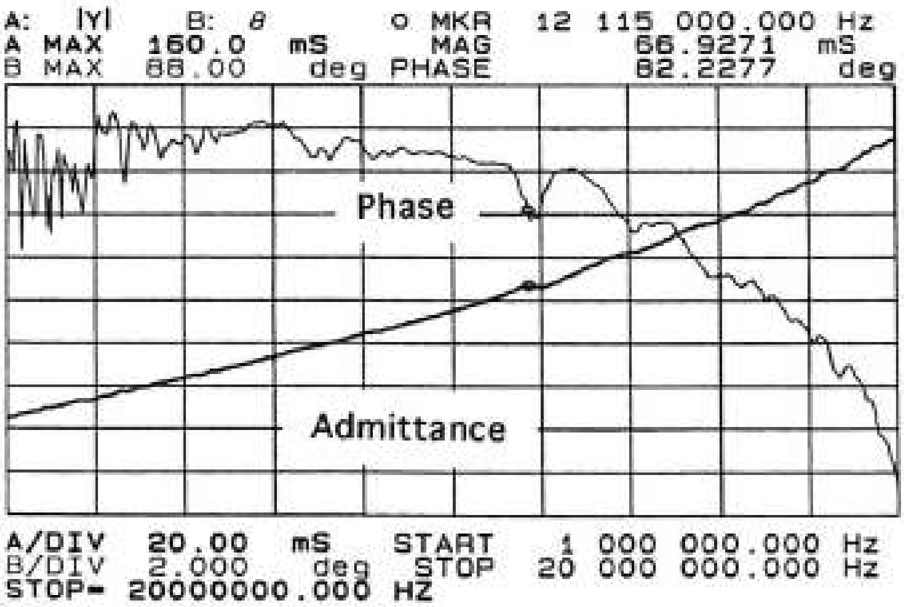

Figure 3.16(b)

Admittance and Phase Plot of a PZT Spherical Transducer

Showing the Thickness Mode

The large rise in the admittance between 15 and 20 MHz is the result of an LC electrical resonance in the system which tends to drown out the response of the high frequency thickness mode, which is not very strong. Special fixtures were made from very low resistance PC board in an attempt to alleviate the problem. The fixtures helped to push the LC resonance to a higher frequency (>25 MHz), however, the rise is still apparent.

It can be seen in Table 3.4 that some of the spheres exhibit no detectable wall thickness resonance. This is attributed to the wide variation in wall thickness within an individual sphere, as described in the statistical sphere evaluation. A large variation in wall thickness within a sphere will cause the peak to spread so much that it is virtually undetectable.

3.2.5 Submerged Impulse Response

Pulse - echo response testing was performed on the PZT spherical transducers at Echo Ultrasound in Reedsville, PA, to evaluate the spheres potential as biomedical imaging transducers. The test setup is shown schematically in Figure 3.17.

The testing procedure is as follows. The spherical transducer is submerged in the water tank, and driven at an arbitrary frequency and amplitude by the 5052UA. The signal from the transducer is then focused on a reflector with a 150° spherical section which was 5.72 cm in diameter. An electrical impulse supplied by the Panametrics 5052UA is then sent to the transducer, which also triggers the Tektronics TDS 520 oscilloscope. The transducer sends an acoustic wave through the water, which is in turn reflected by the reflector. The wave is then sent back to the transducer and converted back to an electrical signal. The response signal is captured by the TDS 520 and sent to an IBM PC where the data is manipulated using Echo ATS software. A fast fourier transform (FFT) response is then generated by the computer, allowing the frequency and bandwidth of the transducer to be evaluated.

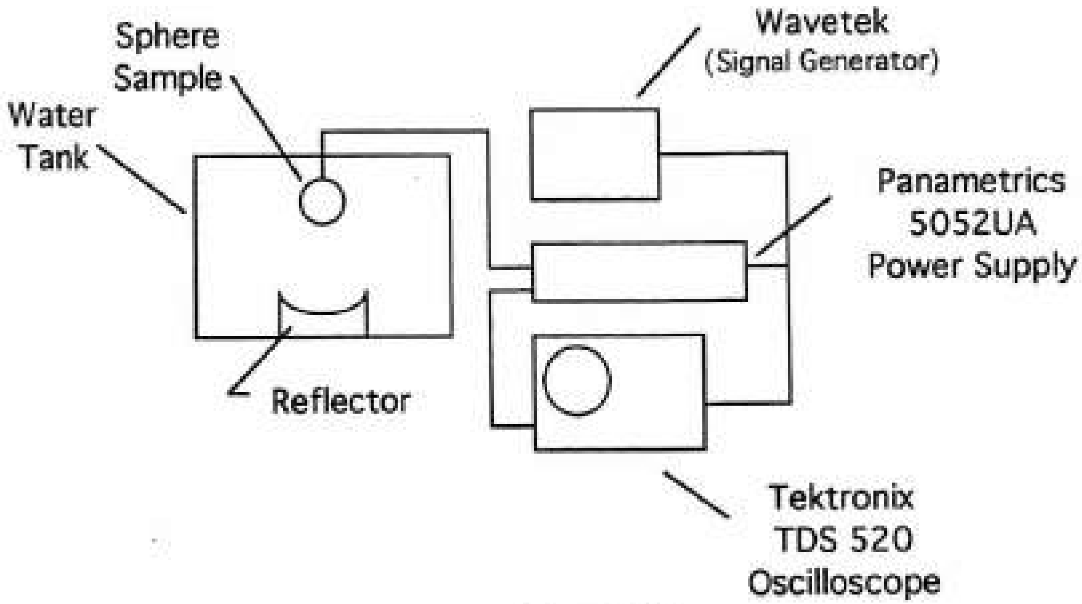

Figure 3.17

Pulse-Echo Response Test Setup

The impulse response characteristics of the spherical transducers show some variation in results, again attributed to non-uniform shape and variation in wall thickness. A good response from a PZT spherical transducer can be seen in Figure 3.18. A typical response from a commercially available ultrasonic imaging composite transducer which has been optimally backed and 1/4 waved can be seen in Figure 3.19 for comparison. Note that the spherical transducer is neither backed to dampen spurious modes, nor 1/4 waved to optimize transmittance of the wave. These are reasons for the imperfect response from the spherical transducers. Improvements in the sphere response can be expected with further investigations in backing materials and 1/4 wave phenomena.

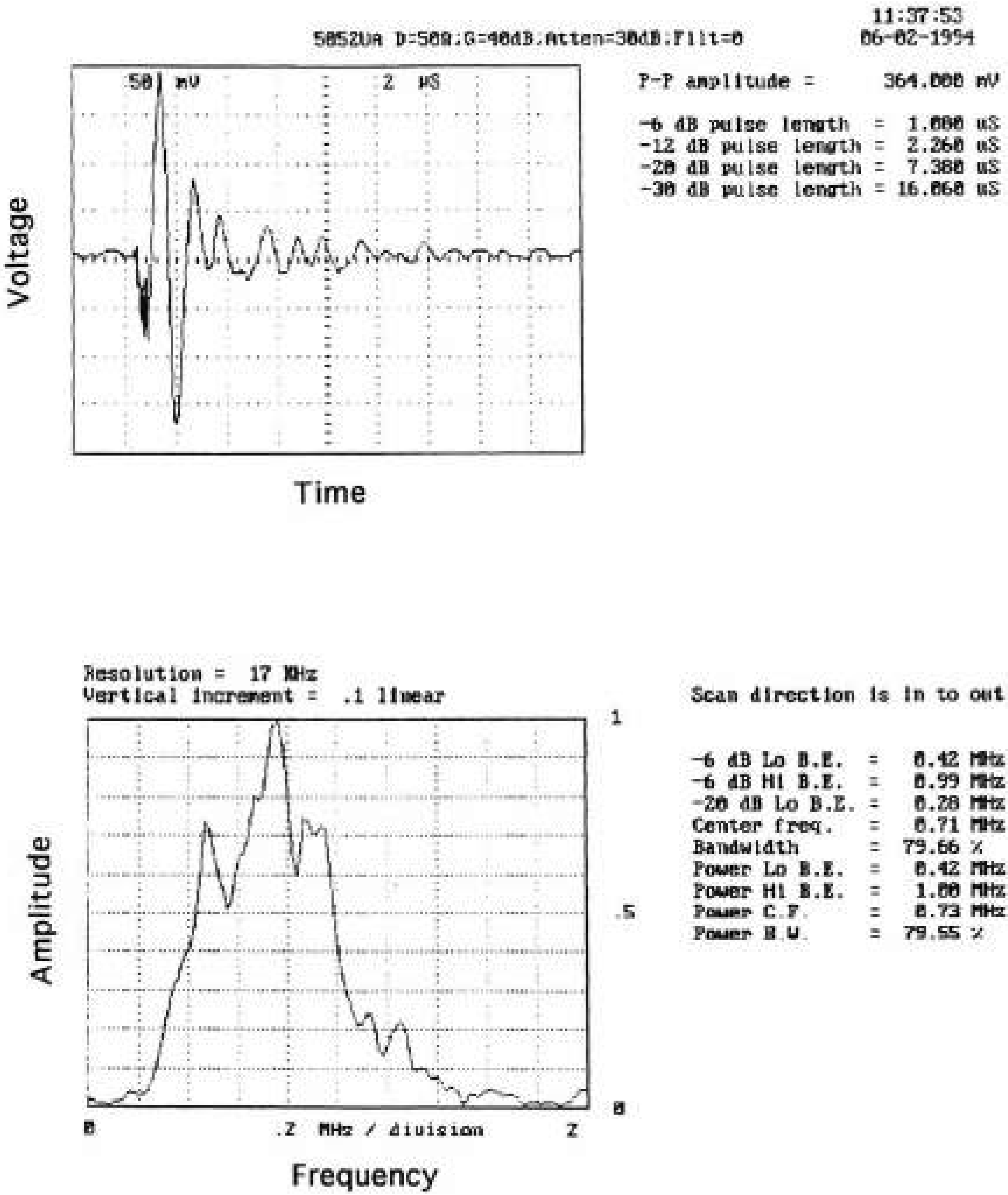

Figure 3.18

Underwater Impulse Response of a PZT Spherical Transducer

(Echo Ultrasound)

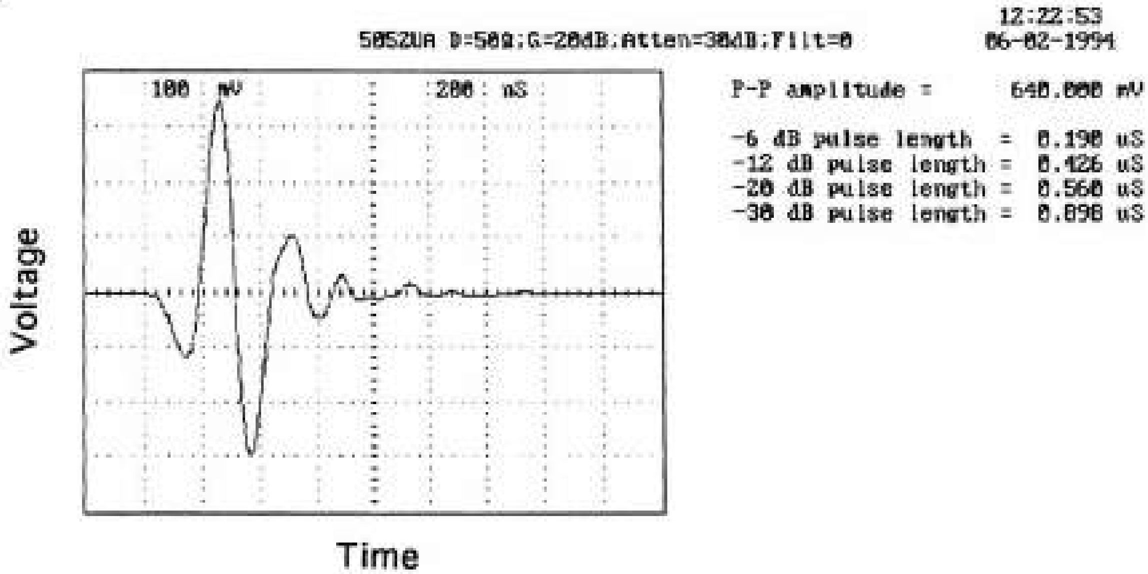

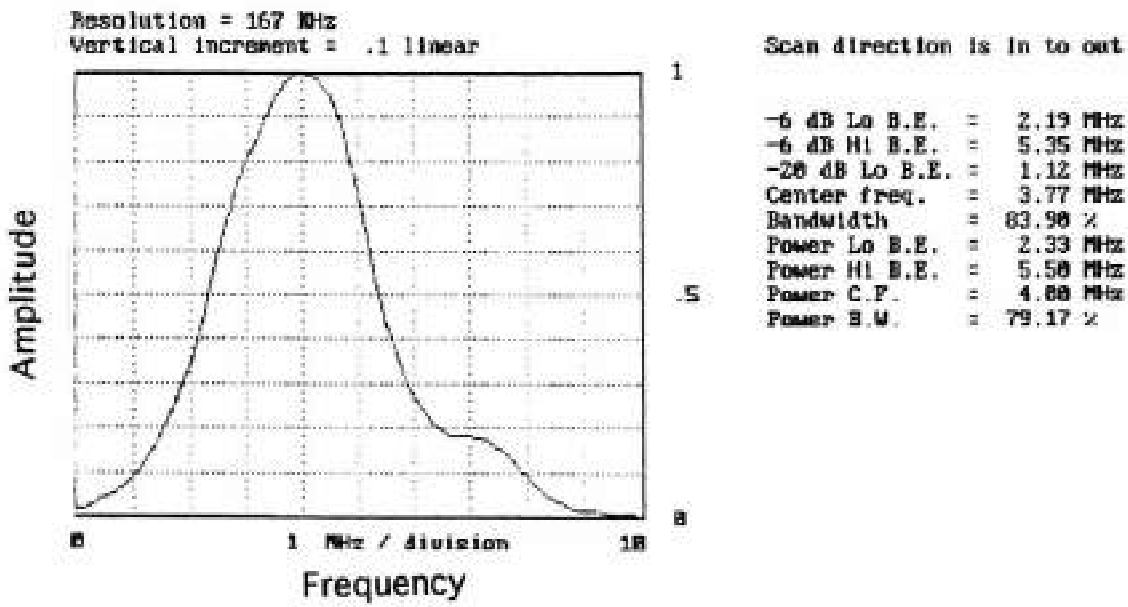

Figure 3.19

Underwater Impulse Response of a Commercially Available Ultrasonic Imaging Composite Transducer (Echo Ultrasound)

From the response of the spherical transducer in Figure 3.18, it can be seen that the response is due primarily to the breathing mode resonance of the transducer, as the center frequency of the response is 710 KHz. The high frequency thickness mode response can only be seen at the leading edge of the response, and is quickly dampened. Again, this can be attributed to the large variation in the sphere wall thickness. The bandwidth of the sphere response is 79.6%, which is nearly the quality of an imaging transducer. However, the frequency is too low for many biomedical ultrasound applications.

The center frequency of the commercially available transducer is at 3.77 MHz and the bandwidth is 83.9%. This frequency is much more desirable for biomedical ultrasound imaging. In order for the spheres to compete with this type of composite transducer for imaging, the variation in wall thickness must be reduced to 5-10% (Kunkel, 1994). Cochran et al. (1994) have reported that by optimizing the fabrication procedure, it is possible to achieve such a tolerance level in hollow sphere ceramics produced by the Torobin process.

Reducing the size of the sphere to achieve a higher frequency breathing mode is not a viable solution. The outside diameter of the hollow sphere would have to be reduced to 0.4 mm to achieve a 3.5 MHz breathing mode resonance, and the current fabrication technology does not accommodate sizes this small.

CHAPTER 4

CONCLUSIONS

4.1 SAMPLE PREPARATION

It was determined that a suitable fabrication procedure had been achieved through evaluation of the last batches of PZT hollow sphere transducers. Yield for the last two batches is 90% (9 of 10) and 100% (12 of 12), respectively. The improved fabrication procedure would allow for a large number of spheres to be produced in a cost effective manner.

Although significant improvements were achieved in the fabrication procedure, there are areas in which further investigation is desirable. The most important of these being improvements in the application procedure, quality, and uniformity of the inner electrode. The current procedure allows the electrode to dry from top to bottom, creating thick and thin electrode areas. Since the sphere walls are quite thin, the mass loading caused by a non-uniform electrode could cause variance in the resonance modes of the spherical transducers.

Another area of concern is the integrity of the bond between the ceramic sphere walls and the silver inner electrodes, since the electrode is simply allowed to settle on the wall and dry as opposed to being physically applied. Any pockets of air trapped within the surface texture of pores in the ceramic will affect the dielectric properties in much the same way that the previously discussed inner porosity would affect them, and may be an additional explanation for the low dielectric constant of the spheres. Suggestions for improvements in achieving an inner electrode are discussed in the following Future Work section.

4.2 POWDER EVALUATION

A time-temperature matrix was investigated on PZT pellets pressed from the same batch of UPI PZT 501A powder used for the fabrication of the PZT hollow spheres. Dielectric and piezoelectric data was collected on the disks at each firing time/temperature combination in the matrix. The data showed that the optimum firing time/temperature combination for sintering was 1285°C for 90 minutes. Thus, a time/temperature combination of 1285°C for 90 minutes was chosen for the PZT spheres.

The data also showed that the dielectric and piezoelectric properties of the disks fired at the optimum schedule were in the range of the values specified by the manufacturer of 1850 for the dielectric constant and 400 pC/N for the piezoelectric d_{33} coefficient.

4.3 STATISTICAL SPHERE EVALUATION

A sink-float test was developed to separate imperfect green PZT spheres before going through the remaining fabrication procedures. Eighty percent of the green spheres failed the sink-float test. Approximately 50% of the spheres had visible holes and cracks, therefore the sink float test proved useful in removing the remaining 30% of the flawed spheres which had defects undetectable during visual inspection. The sink-float test is also much less time consuming, as many spheres can be screened simultaneously.

Weight, size, shape and weight loss during sintering was monitored on a batch of 100 spheres in this investigation. From the data obtained, calculations were made to give insight on the inside radii, wall thickness, and effective density of the PZT hollow spheres. The results of the statistical sphere evaluation are summarized in Table 4.1

Table 4.1

Summary of the Data Obtained in the Statistical Sphere Evaluation

Parameter Measured	Measured Average	Std. Dev.
Weight of Green PZT Spheres	14.2 mg	0.44 mg
O.D. of Green PZT Spheres	3.31 mm	0.037 mm
Spherodicity of Green Spheres	1.88 %	----
Weight of Sintered PZT Spheres	13.8 mg	0.43 mg
O.D. of Sintered Spheres	2.76 mm	0.039 mm
Spherodicity of Sintered Spheres	2.28%	----
Shrinkage (During Sintering)	16.6 %	----
I.D. of Sintered Spheres	2.60 mm	0.044 mm
Sintered Sphere Wall Thickness	79.4 µm	0.37 µm
Effective Density	1.25 g/cc	0.068 g/cc

Weight loss of the PZT spheres was monitored during burnout and sintering. The data shows a weight loss of 3.1% during burnout, corresponding to the amount of binder added in fabrication to aid in shape retention. No appreciable weight change was noted between the burned out and sintered weight of the spheres, signifying no detectable weight loss during sintering.

Wall thickness variation within individual spheres was evaluated by observing the cross-section of twenty five hemispheres. The investigation revealed a typical wall thickness variation within a sphere to be 3 to 1. This large variation leads to the extremely broad and weak (often undetectable) wall thickness resonance in the admittance spectra for the spheres (Section 3.4.4), and the lack of the high frequency portion in the pulse-echo impulse response of the PZT spherical transducers.

It can be seen from Table 4.1 that the aspherodicity of the spheres increased as a result of the firing procedure. This is probably a result of the spheres slumping during sintering. It is suggested that a fixture be designed for firing the spheres to alleviate this problem in the future.

Another observation in the wall thickness evaluation was the presence of large pores and cracks along the thin walls, and areas of low density in the PZT sphere walls. The pores in the sphere walls were concentrated in the thick wall areas, while the cracks were typically observed in the thin wall sections of the spheres. It was determined that the poor dielectric properties reported on the spheres in Section 3.4.2 are largely caused by the observed flaws in the sphere walls. Considering mixture rule theory, it only takes a small percentage of voids to affect the dielectric constant of a material markedly.

Possible solutions to the wall thickness variation and wall density problems are discussed in the Future Work section of this thesis.

4.4 CHARACTERIZATION OF PZT SPHERICAL TRANSDUCERS

4.4.1 Dielectric Measurements on Spheres

The average dielectric constant of the PZT spherical transducers was 677. This varies significantly from the value of 1850 reported in the specifications for UPI PZT

501A powder. The variation is attributed to a combination of the low density and porosity of the sphere walls, and the imperfect inner electrodes as described in this chapter in sections 4.2 and 4.3, respectively.

4.4.2 Piezoelectric Measurements

(a) Hysteresis Loops

Values for the remanent polarization (P_r) and coercive field (E_c) were obtained on the PZT spherical transducers. The average P_r was determined as 319 mC/m^2, and the average E_c as 2.1 MV/m. The average P_r of the PZT control pellets is 364 mC/m^2, and the average coercive field is 0.93 MV/m. The 12% reduction in P_r and the 120% increase in E_c can be tied to the imperfect inner electrodes, and the presence of porosity in the sphere walls.

(b) Hydrostatic Measurements

Hydrostatic measurements were taken on the spherical transducers as described in section 3.4.3 (b). The average values of d_h versus pressure for the spheres is between 957 and 526 pC/N. A table listing the d_h constants of other hydrophone materials is shown in Table 4.2 for comparison. The significantly higher values of d_h for the spheres are due to stress magnification as a result of the transducer geometry, and the fact that the hollow spheres are backed with air which allows for significantly more deformation than bulk materials can achieve.

Table 4.2

d_h Coefficients of Composite Hydrophone Materials

Composite Material	d_h (pC/N)
0-3 Composite: PbTiO3-Chloroprene Rubber	35
1-3 Composite:PZT rods - spurs epoxy w/brass Electrode	45
1-3-0 Composite: PZT rods - foamed (REN)	87
3-3 Composite: PZT - silicone rubber (Burps)	180
Metal - Ceramic Composite: Moonie transducer	1000
PZT hollow sphere transducers	675

4.4.3 RESONANT FREQUENCY

As described in sections 1.4 and 3.4.4, the primary and secondary vibration modes of hollow spherical shells are the breathing mode and wall thickness mode, respectively. With the average values for diameter and wall thickness arrived at in the statistical sphere evaluation, expected values for the frequencies can be calculated.

The average resonant frequency of the primary breathing mode of the spherical transducers is 707 KHz. The variance is close to that observed in the average outer diameter of the spheres of approximately 5%, as the resonant frequency of the breathing mode depends primarily on the average radius of the spherical shell.

The average resonant frequency of the wall thickness mode of the transducers is 14.9 MHz. The larger variance in this data is a result of the larger variance in wall thickness of the PZT spheres, as the resonant frequency of the thickness depends primarily on the wall thickness of the spherical shell. From Table 3.9 it can be seen that some of the spheres do not exhibit a distinguishable high frequency wall thickness mode in the resonance spectra. This is due to the large wall thickness variation (3 to 1) described in the statistical sphere evaluation.

Since the average outer diameter variation in the spheres is only 5% using the current fabrication method, the breathing mode resonance of the transducers is predictable and repeatable. The breathing mode resonance peak in the admittance plots for the spheres is strong and fairly sharp, making the spherical transducers useful in applications where the breathing mode resonance would be utilized, such as non-destructive testing and hydrophone applications.

The wide variance in wall thickness within a sphere (300%), and between different spheres (11%) make the wall thickness mode resonance of the spheres less predictable and more difficult to detect. Thus, the current fabrication method for the spheres would have to be improved to provide hollow spheres with uniform wall thickness to make them useful in applications where the high frequency thickness mode would be utilized, such as in biomedical ultrasound imaging. This point is addressed again in the next section, where pulse-echo response testing is discussed.

4.4.4 SUBMERGED IMPULSE RESPONSE TESTING

Results from pulse-echo response testing show a strong response from the breathing mode of the transducers, but little response from the wall thickness mode. This is to be expected as a result of the wide variation in wall thickness within a given sphere.

The sphere's breathing mode response produces a reasonably clean response, given the fact that the PZT spheres are hollow and backed with air. Some of the spheres have a bandwidth near 80%, which is approaching the quality of an imaging transducer. Therefore, the current spheres are potentially useful in applications which require frequencies in the KHz range, such as non-destructive testing and non-destructive evaluation. This frequency, however, is too low for biomedical ultrasound imaging, where frequencies in the MHz range are desirable for improved resolution.

In order for the spheres to possess potential for biomedical imaging, the wall thickness mode has to be sharp and strong. In order to improve the quality of the wall thickness resonance, the spheres would have to have a wall thickness variation of approximately 5%. This concern is currently being addressed by the sphere manufacturer. In the current condition the spheres could be used as guidance beacons for invasive surgery where the location of the catheter needs to be established. Guidance beacons simply need to emit a known frequency which can be detected by the location monitor placed against the patient's body.

CHAPTER 5
FUTURE WORK

5.1 INTRODUCTION

This thesis describes a fabrication procedure for producing PZT hollow sphere transducers in a cost effective manner and the characterization of these spherical transducers to evaluate their potential for use as miniature hydrophones and biomedical sensors. Although the PZT spheres possess some superior characteristics when compared to other designs, there are still many aspects of the transducers which could benefit from further investigations. Some of the foreseen areas for improvement are discussed in this chapter.

5.2 SPHERE WALL THICKNESS VARIATION

A large variation in the wall thickness within individual spheres was observed in this investigation. This wall thickness variation degraded the high frequency thickness mode of vibration of the spherical transducers, causing the resonance peaks of the mode to be either weak and broad, or undetectable. Investigation of new methods for green sphere fabrication should be carried out in an attempt to create spheres with uniform walls (approximately 5% variation, or less). Spheres with uniform wall thickness should have strong sharp peaks for the high frequency thickness mode of vibration. This would allow the PZT spheres to be useful in biomedical ultrasound applications where high frequency signals are used in imaging to increase resolution.

5.3 FABRICATION PROCEDURE

5.3.1 INNER ELECTRODE IMPROVEMENTS

Achieving a uniform inner electrode with good integrity and adhesion to the thin sphere walls should be investigated. The low dielectric constants reported in this investigation for the spheres may be due, in part, to poor inner electrode contact with the sphere walls. A uniform electrode coating will also improve the sharpness of the resonance peaks by reducing uneven mass loading of the thin sphere walls. Examples of electroding methods which could be investigated are a reduction/oxidation method to achieve a conductive layer at the inner sphere wall with compositions other than PZT which have sufficient conductivity when reduced, electroless plating techniques, and electrostatic spraying of conductive paint.

5.3.2 Drilling Procedure

The method used in this investigation for achieving the access holes through the thin PZT walls was to mount them in a low melting point polymer material and drill them with a small bit. This method was successful, however, it was time consuming and occasionally formed small stress cracks at the small hole. A more efficient manner to achieve better quality holes should be investigated. Some possibilities are the use of lasers, acid etching, and abrasion methods.

5.4 ACOUSTIC IMPEDANCE MODIFICATIONS

Previous work has been completed showing that the acoustic impedance of piezoelectric transducers can be tuned with polymer coatings and backing materials

(Grewe, 1989). Investigations should be completed on PZT hollow sphere transducers with different coatings and backing materials. Spheres could be back-filled with various density fillers or polymers to adjust attenuation and ring down time in the transducers. Quarter wave coatings should also be investigated to improve coupling between the PZT spherical transducers and the water or human tissue.

5.5 ADDITIONAL MATERIALS

Other materials should be investigated, in conjunction with the other improvements, in the spherical transducer configuration to evaluate their potential for specialized applications. Examples of materials which could be tried are the relaxor ferroelectric PMN-PT for its high electrostrictive coefficients, and $PbNb_2O_6$ which is an excellent hydrophone material. It is possible that these materials, along with many others, may find a niche in certain applications when produced as tiny hollow spherical transducers.

REFERENCES

Berlincourt, D. A., D. R. Curran, and Hans Jaffe, "Piezoelectric and Piezomagnetic Materials and Their Function in Transducers", in Physical Acoustics, Volume 1, part A, Ed by W. P. Mason, Academic Press, NY (1964).

Chapman, A. T., J. K. Cochran, M. K. Adicks, G. E. Carlson, P. R. Chu, J, H. Chung, R. B. Clancy, T. R. Ford, S. D. Furlong, T. J. Hwang, C. M. Moore, M. J. Shapiro, "Thin-Wall Hollow Spheres from Slurries", Poster Presentation, The Annual Review Meeting, Advanced Industrial Concepts Materials Program, DOE, Albuquerque, NM, June, (1991).

Chapman, A. T., J. K. Cochran, J. M. Britt and T. J. Hwang, "Thin-Wall Hollow Spheres from Slurries", DOE-ECUT Program, ONRL Subcontract 86X-22043C, Annual Reports (1987).

Chu, P. R. , and J. K. Cochran, "Coaxial Nozzle Formation of Hollow Spheres from Liquids I: Model", Manuscript 194543P, submitted to the Journal of the American Ceramic Society, July (1993)

Clancy, R. B., T. H. Sanders, and J. K. Cochran, "Fabrication of Thin-Walled Hollow Nickel Spheres and Low Density Syntactic Foams", in Light Weight Alloys for Aerospace Applications II, Ed. by E. W. Lee and N. J. Kim, The Minerals, Metals, and Materials Society, pp. 477-485, (1991).

Cluley, S. R., B. J. Brener, L. H. Hollier, D. E. Eisenbud, M. Ferarra-Ryan, A. Villanueva, V. Parsonnet, and D. Vilkomerson, "Ultrasound-Guided Balloon Angioplasty is a New Technique for Vascular Surgeons", The American Journal of Surgery, **162**, pp. 117-121, (1991)

Cochran, J. K., et al., Personal communication at the poster session for The American Ceramic Society, Indianapolis, Indiana, April, (1994).

Cochran, J. K., G. E. Carlson, P. R. Chu, J. H. Chung, R. P. Gonzales, T. J. Hwang, A. S. Jenson, and L. A. Touryan, "Thin Wall Hollow Spheres From Slurries", Materials Engineering, Georgia Institute of Technology, Poster Presentation for the Advanced Industrial Concepts Materials Program, Department of Energy, Pleasanton, CA, (1992).

Gentilman, R., L. Bowen, D. Fiore, H. Pham, and W Serwatka, Material Systems Inc., "Sonopanel 1-3 Piezocomposite Panels for Sonar and Active Surface Control", Presentation at ONR Transducer Materials & Transducers Workshop, The Pennsylvania State University, April 4, 1995.

Grewe, M. G., Acoustic Matching and Backing Layers for Medical Ultrasonic Transducers, M.S. Thesis, The Pennsylvania State University, May (1989).

Gururaja, T. R., Piezoelectric Composite Materials for Ultrasonic Transducer Applications, Ph.D. Thesis, The Pennsylvania State University, May (1984).

Holman, R. L., and R. M. Fulrath, "Intrinsic Nonstoichiometry in the Lead Zirconate-Lead Titanate System Determined by Knudsen Effusion", Journal of Applied Physics, Volume **44**, No. 12, December (1973).

Ivey, L. E., "NRL-USRD Series F42 Omnidirectional Standard Transducers", Underwater Sound Reference Detachment, Naval Research Laboratory, Orlando, Florida, (1979).

Jaffe, B., W. R. Cook Jr., and H. Jaffe, Piezoelectric Ceramics, pp. 135-183, R. A. N. Publishers, Marietta, Ohio (1971).

Kunkel, H., Senior Design Engineer, Echo Ultrasound, Inc., Reedsville, P.A., Personal communication, May, (1994).

Meyer, C. R., E. H. Chiang, K. P. Fechner, D. W. Fitting, D. M. Williams, and A. J. Buda, "Feasibility of High-Resolution Intravascular Ultrasonic Catheters, Radiology, 168, No. 1, pp. 113-116 (1988).

Meyer, Jr., R., H. Weitzing, Q. Xu, Q. Zhang, R. E. Newnham, and J. K. Cochran, "Lead Zirconate Titanate Hollow-Sphere Transducers", Journal of the American Ceramic Society, 77(6), pp. 1669-1672, March (1994)

Neville, R. F., A. L. Bartorelli, A. N. Sidawy, Y. Almagor, B. Potkin, M. B. Leon, "An In Vivo Feasibility Study of Intravascular Ultrasound Imaging", The American Journal of Surgery, **158**, pp. 142-145 (1989).

Pandian, N. G., "Intravascular and Intracardiac Ultrasound Imaging: An Old Concept on the Road to Reality", Circulation, **80**, No. 4, pp. 1091-1094, (1989).

Romanenko, E. V., "Miniature Piezoelectric Ultrasonic Receivers", Soviet Physics Acoustics, Vol. **3**, pp. 364-370 (1957).

Silk, M. G., "Ultrasonic Transducer for Nondestructive Testing", Adam Hilger Ltd., Bristol (1984).

Timoshenko, S. and J. N. Goodier, Theory of Elasticity, McGraw-Hill Book Company, Inc., New York, (1951).

Torobin, L. B., U. S. Patent 4,671,909 (1987)

Vilkomerson, D., B. Gardineer, and H. Hojeibane, "Quasi-Omnidirectional Transducers for Ultrasonic Electro-Beacon Guidance of Invasive Devices", SPIE Vol. **1733**, pp. 154-165, (1992).

Wells, P. N. T., Biomedical Ultrasonics, Academic Press, London (1977).